Chapter 2
Properties of Bulk Zirconium Hydrides

2.1 Hydride Phase Compositions, Lattice Structure and Parameter Determinations

Bulk zirconium hydrides refer to hydrides of macroscopic dimensions in which the zirconium starting material has been completely converted to a single or a mixture of zirconium hydride phases. The need for the study of such bulk material is particularly important in the determination of lattice parameters to ensure that these are obtained for elastically unconstrained material and are, thus, representative of the stress-free state of the lattice.

It turns out that there are large differences between the unconstrained lattice parameters of the parent α-Zr phase and a given hydride phase as well as between different hydride phases. These large differences can result in significant coherency stresses in and around hydride precipitates. Such coherency stresses have important effects on phase relationships. There have been various theoretical interpretations of the effects of these coherency strains on hydrogen solubility in the α-Zr phase at the $\alpha/(\alpha + \delta)$ solvus boundary (see Chap. 6). These interpretations have been used to rationalize the experimental observation that hydrogen solubility at this phase boundary is history dependent and differs substantially depending on whether the state of the system is one of formation or dissolution of the hydrides. Not quantitatively assessed for metal-hydrogen and particularly the Zr-H system before this publication is that these coherency effects manifest themselves also in differences in the $(\alpha + \delta)/\delta$ phase boundary composition, even when hydrogen absorption is carried out to complete conversion between parent and solid hydride phase and all of the coherency stress effects have disappeared. The reason is discussed in detail in Chap. 7.

The constraint effects resulting from the large lattice mismatches between phases create large stresses in the hydride and matrix, well exceeding the elastic limits of the materials. These high stresses can be relieved through internal microscopic relaxation mechanisms such as those of thermal diffusion of the Zr

M. P. Puls, *The Effect of Hydrogen and Hydrides on the Integrity of Zirconium Alloy Components*, Engineering Materials, DOI: 10.1007/978-1-4471-4195-2_2,

atoms at the hydride-metal interface and/or of plastic deformation of the hydride and metal phases. If this is not the case, cracks or pores could form during the formation (or dissolution) stages of the hydrides. This could occur if the rate of hydrogen ingress and/or of cooling of the specimen is too rapid compared to the rate at which the foregoing internal relaxation processes would be able to relieve the associated internal stresses. These rather complex aspects of hydride-metal "equilibrium" are discussed in more detail in Chaps. 6–8 dealing with the $\alpha/(\alpha + \delta)$ and $(\alpha + \delta)/\delta$ solvus relations where it will be shown that in this type of system, at temperatures where full or partial coherency stresses are generated and maintained between any two phases, only metastable equilibrium states are possible and these metastable states have compositions that are different from those expected if true thermodynamic equilibrium could have been achieved. Hence, the phase boundary compositions at the $(\alpha + \delta)/\delta$ solvus given in this chapter—since they are taken from early published literature on this topic when workers were unaware of these hysteresis effects—do not explicitly account for any possible effect of hysteresis on their compositions.

Studies of the phase constitution of the Zr-H system have identified three zirconium hydride phases, γ, δ and ε, differing in their crystallography and hydrogen composition. These phases have, respectively, nominal stoichiometric compositions of ZrH, $ZrH_{1.5}$ and ZrH_2. It seems, however, that only the γ-hydride phase is truly stoichiometric, having a one-to-one ratio of hydrogen to zirconium atoms while the other two hydrides can exist over a range of hydrogen compositions.

2.1.1 Crystallographic Properties of the γ-Hydride Phase

Most measurements have indicated that γ-hydride has an ordered, tetragonal structure (space group $P4_2/n$) with room temperature lattice parameters, $\boldsymbol{a_0} = 4.596$ Å and $\boldsymbol{c_0} = 4.969$ Å, resulting in a unit cell volume, $\boldsymbol{a^2c}$, of 103.72 $Å^3$ [24]. Since there are four Zr atoms in a unit cell this results in an atomic volume (Wigner–Seitz cell volume), Ω^{γ}_{Zr} or $\bar{V}^{\gamma}_{Zr}$, of 25.93 $Å^3$/(atom Zr-γ) or 15.62×10^{-6} m^3/(mol Zr–γ), respectively. The hydrogen atoms in this structure occupy tetrahedral sites on alternate (1 1 0) planes. The Zr atoms are found at the (1/4 1/4 1/4) sites while the hydrogen atoms occupy the (0 0 0) or (0 0 1/2) sites. Results from inelastic neutron scattering studies of ZrD show that the γ-phase structure actually has a small orthorhombic distortion, space group Cccm (No. 66) with $\boldsymbol{a_0} = 4.549$ Å, $\boldsymbol{b_0} = 4.618$ Å, and $\boldsymbol{c_0} = 4.965$ Å [16]. The orthorhombic structure of γ-ZrH(D) is consistent with that of γ-TiH(D) obtained previously [2, 17, 19, 21]. The difference between the lattice parameters, $\boldsymbol{a}$ and $\boldsymbol{b}$, is, however, small (1.5 %) and, as Kolesnikov et al. [16] point out, this small difference would not be detectable by conventional neutron diffractometers.

It should also be noted that these results were obtained in specimens having an overall composition of $ZrD_{0.28}$ consisting (according to the neutron scattering results) of α-, γ-, and δ-hydride and compositions given as follows:

$$ZrD_{0.28} \leftrightarrow 0.718(\alpha\text{-}ZrD_{0.001}) + 0.269(\gamma\text{-}ZrD_{0.98}) + 0.013(\delta\text{-}ZrD_{1.2}) \quad (2.1)$$

From the proportions and compositions of the phases in the specimen given by Eq. 2.1 it is evident that the proportion of the δ-phase present is very small. However, given the much larger amount of α-Zr phase present compared to the γ-phase and the very small amount of the δ-phase, one can surmise that the γ-phase would have been dispersed as precipitates in the α phase (unfortunately no metallographic evidence was provided to show the structure and orientation of these precipitates). This means that the γ precipitates would be under some compression, possibly decreasing their lattice parameters relative to their values at zero stress (but not necessarily all of them equally). The magnitudes of the three orthogonal normal stresses in the hydride precipitates would depend on their shapes and transformation strains. It is shown in Chap. 3 that γ-hydride formation in the α-Zr phase likely occurs via an invariant plane strain transformation. This implies that the net transformation involves only a dilatation normal to the invariant habit plane (except for possibly also a small uniform dilatation in the plane) plus shears parallel to this plane. The precipitate shape of minimum energy for such a transformation would be a plate-shaped precipitate having a small thickness-to-length ratio. For such a hydride shape and transformation strains, the stress in the plate-normal direction, $\boldsymbol{c}$, would be negligible along most of the length of the plate-shaped precipitate. However, because of the considerable dilatational transformation strain of $\sim$0.12 in that direction, the Poisson's contraction would generate large compressive stresses in the in-plate directions, $\boldsymbol{a}$ and $\boldsymbol{b}$, of these γ-hydride precipitates. The reduction in lattice spacing as a result of these compressive stresses may not be equal if the plate has dimensions that are different in the $\boldsymbol{a}$ and $\boldsymbol{b}$ direction, which may account for Kolesnikov et als' finding of orthorhombic symmetry for the embedded γ-hydride precipitates. Because of the foregoing concerns regarding the experimental results of Kolesnikov et al. and the small differences between the $\boldsymbol{a}$ and $\boldsymbol{b}$ lattice parameter values, we will continue to refer to the lattice structure of the γ-hydride phase as being face centred tetragonal (fct) in the following.

It should be noted that the foregoing considerations could also apply to the lattice parameter determinations of the γ-hydride phase made by other workers, since this phase is almost always found in an embedded state, as discussed in more detail further on. However, using powder X-ray diffraction techniques the low penetrating power of the X-rays compared to that of neutrons, plus the use of powder specimens, which means that any γ-hydride precipitates would not be far from a free surface, would mitigate these lattice constraint effects because the lattice spacing of only those γ-hydride precipitates that are close to the surface would be measured, for which the constraint effects as a result of their embedment would be minimized.

Before continuing with a description of the lattice properties of the γ-hydride phase, it is convenient for the treatment of their thermodynamic properties further on to define a concentration variable, $\theta_{\text{pha}} = r_H/\beta_{\text{pha}}$, where β_{pha} is the number of available (or preferred) interstitial sites per Zr atom sites in the phase "pha" and r_H is the ratio of the number of hydrogen atoms to Zr atoms in the crystal in the phase

being considered. (To avoid cumbersome notation in some cases, where the meaning is clear the subscript *"H"* is omitted from r_H).

The hydrogen molar or atomic volume in the γ-hydride phase, $\bar{V}_H^{\gamma-\text{hyd}}$ or $\Omega_H^{\gamma-\text{hyd}}$, respectively, is defined as the difference between the molar or atomic volume of zirconium in the γ-phase and in the α-Zr phase at infinite dilution of H, viz.,

$$\bar{V}_H^{\gamma-\text{hyd}} = \frac{\bar{V}_{\text{Zr}}^{\gamma-\text{hyd}} - \bar{V}_{\text{Zr}}^{\alpha-\text{Zr}}}{\beta_{\gamma-\text{hyd}}} \quad \text{or} \quad \Omega_H^{\gamma-\text{hyd}} = \frac{\Omega_{\text{Zr}}^{\gamma-\text{hyd}} - \Omega_{\text{Zr}}^{\alpha-\text{Zr}}}{\beta_{\gamma-\text{hyd}}} \tag{2.2}$$

and similarly for the δ-hydride molar or atomic volumes. The value of $\beta_{\text{pha}} \equiv \beta_{\gamma-\text{hyd}}$ in Eq. 2.2 depends on which hydride is being considered. In the case of the γ-hydride crystal structure, experimental evidence shows that only half of the two available preferential tetrahedral interstitial sites per zirconium atom are actually ever occupied at any one time by hydrogen atoms. Hence, $\beta_{\gamma-\text{hyd}} = 1$. On the other hand, for δ-hydride it would appear that although there are again two available preferential tetrahedral interstitial sites per zirconium atom, the composition of this hydride seems centred at a stoichiometric composition of 1.5 suggesting that $\beta_{\delta-\text{hyd}} = 1.5$. However, the equilibrium composition of the hydride, which is given by r_H, can vary somewhat in this case since r_H decreases to values less than $\beta_{\delta-\text{hyd}} = 1.5$ as the temperature is raised from ambient to the eutectoid temperature.

Now, the room temperature lattice parameters of the hcp α phase are $\boldsymbol{a_0} = 3.231$ Å and $\boldsymbol{c_0} = 5.146$ Å [16]. The unit cell volume of the α-Zr phase, given by $3\boldsymbol{a}^2\boldsymbol{c}\sin 60°$ (or $\sqrt{3}/4\boldsymbol{a}^2\boldsymbol{c}$), is thus 139.57 Å^3. There are six Zr atoms in a unit cell of α-Zr; therefore the atomic or molar volume of α-Zr (Wigner–Seitz cell volume), denoted by $\Omega_{\text{Zr}}^{\alpha-\text{Zr}}$ or $\bar{V}_{\text{Zr}}^{\alpha-\text{Zr}}$, is the unit cell volume divided by six, yielding 23.26 Å^3/(atom Zr) or 14.01×10^{-6} m^3/(mol Zr), respectively. The experimental results of Kolesnikov et al. indicate that r_H is close to unity in the γ-hydride phase. The molar volume, $\bar{V}_H^{\gamma-\text{hyd}}$, of H in γ-hydride given by Eq. 2.2, then, is 1.61×10^{-6} m^3/(mol H).

2.1.2 Phase Relationships, Phase Stability, and Hydrogen Compositions in the δ- and γ-Hydride Phases at the (α + δ)/δ Phase Boundary

Over the years, there have been numerous experimental observations and theoretical arguments put forth in the literature concerning the nature of the γ-hydride phase, particularly its thermodynamic stability. With reference to this debate, which is dealt with further in Chap. 6 in which the $\alpha/(\alpha + \delta)$ and $(\alpha + \delta)/\delta$ solvus relations are explored, it should be noted that despite some recent concerted attempts toward this goal [6, 16], no one has, so far, been able to produce bulk specimens consisting entirely of the γ-hydride phase, even when hydrogenating specimens to an overall composition equal to the observed stoichiometric composition of this phase,

i.e., ZrH_r or ZrD_r, with $r = 1$. This inability to produce bulk specimens consisting entirely of the γ-hydride phase appears to be an important indication that this phase is metastable throughout the temperature range below the eutectoid temperature. Generally, what has been observed in hydrogenating Zr metals to overall hydrogen compositions below a range from $ZrH_{1.3}$ at the eutectoid temperature to $ZrH_{1.6}$ at room temperature—at and above which composition only the single δ-hydride phase is present until the ε-hydride phase field is reached—has consisted of a mixture of either the α-Zr, γ-, and δ-hydride phases, or only of the γ- and δ-hydride phases. These results are described in more detail in the following.

In neutron and X-ray diffraction studies of hydrogenated Zr metal prepared in the form of thin strips or filings from crystal bar purity stock, Sidhu et al. [24] listed the observed phases and their relative proportions in terms of diffraction intensity signals starting from an overall composition range from ZrH_0 to $ZrH_{0.11}$ and ending with the terminal composition range from $ZrH_{1.70}$ to $ZrH_{1.99}$. As the composition of hydrogen was increased, it was inferred from the signal strength data that the starting decomposition of the α-Zr phase resulted in a mixture of γ-hydride and remaining α-Zr phases, with the γ-hydride likely present initially as precipitates within the α-Zr matrix that, up to $ZrH_{1.0}$, evolved into a mixture of predominantly γ- and δ-hydride phases in addition to a small amount of remaining α-Zr phase. At higher H/Zr ratios the α-Zr phase disappeared entirely and the γ-hydride phase became a minority one, likely contained within the δ-hydride phase. Between $ZrH_{1.4}$ and $ZrH_{1.6}$, only the δ-hydride phase was found. Beyond that composition there was a mixture of δ- and ε-hydride phases over a narrow composition range from $ZrH_{1.6}$ to $ZrH_{1.70}$. Above these composition ratios only the ε-hydride phase was observed.

Beck [7] carried out a study of the Zr–H system with the main objective the determination of the hydrogen solubility limit in the δ-hydride phase at the $(\alpha + \delta)/\delta$ phase boundary, since—particularly at room temperature—this composition had been the source of disagreement among investigators. Beck determined the room temperature composition to be at 61.4 ± 0.2 at % H ($r_H = 1.59$) with, as he stated, "…considerable certainty". Beck's confidence in the correctness of this result was based, in part, on the results and interpretation of supporting experimental studies concerning the nature and origin of the γ-hydride phase. All previous workers had found from room temperature measurements that there existed a third phase in the $(\alpha + \delta)$ region which was identified as the γ-hydride phase. To determine whether this phase was metastable, Vaughn and Bridge [28] had carried out high temperature diffraction studies by aging the material at 500 °C for 48 h. They had found that the γ-hydride phase could be eliminated. On the other hand, Eiler et al. [13], using only diffraction measurements taken at room temperature, had found the γ-hydride phase in specimens that, prior to the room temperature diffraction measurements, had been aged for a similar period at 540 °C. Similarly, Gulbransen and Andrew [14] had found evidence in room temperature diffraction measurements of the presence of the γ-hydride phase in specimens that had been hydrogenated several hundred degrees below the eutectoid temperature. In Beck's own studies [7], vycor-encapsulated specimens were aged for 5 days at 500 °C followed by room temperature diffraction studies. These studies found no change in the room

temperature intensities of the powder patterns taken subsequent to the aging treatment compared to those taken before this treatment. Since Vaughn and Bridge [28] were the only workers that had made diffraction measurements at the aging temperature, Beck suggested that a plausible explanation for these combined observations is that the γ-hydride phase had actually disappeared at the aging temperature and then reappeared on cooling to room temperature. On the basis of these results, Beck concluded that the γ-hydride phase must be a metastable phase that is formed on cooling. To determine the reason for its formation during cooling, Beck noted that in a powder X-ray diffraction pattern the relative amounts of phases present is qualitatively proportional to the observed signal strength of the strongest line for each phase. From the data listed in this author's Table 1, he concluded, therefore, that the amount of the γ-hydride phase was clearly proportional to the δ-hydride and not the α-Zr phase. Beck pointed out that the likelihood of the γ-hydride phase being an allotropic modification of the δ-hydride phase is very low given its observed insensitivity to quenching and aging procedures and the relatively high rate of the transformation. Beck, therefore, concluded that γ-hydride is a metastable decomposition phase of δ-hydride rather than of the equilibrium α-Zr phase and which—on the basis of studies of the reaction kinetics—forms continuously as a function of temperature. Beck constructed a model to support this conjecture as follows.

Beck assumed that the γ-hydride phase must have a hydrogen composition intermediate between that of the δ-hydride and α-Zr phases. Beck further conjectured that the actual composition of the γ-hydride phase would have to be ZrH_r, where $r \equiv r_H = 1$, on the basis of its crystal structure, a conjecture that has since been verified by many workers [34]. According to Beck, the structure of the γ-hydride phase is body-centered tetragonal (bct),[1] which he claimed was additionally supported by theoretical intensity calculations showing that the Zr atoms are located at the center of the lattice points. Assuming that the density of the δ-hydride phase must be intermediate between those of the δ-hydride and α-Zr phases, the unit cell would have to be simple bct containing only two metal atoms, ignoring the small contribution that hydrogen would make to the density. As a result, the arrangement of Zr atoms in the δ-hydride phase must be identical to that in the ε-hydride phase. Beck noted that the bct cell can be converted to the face centered cubic cell simply by multiplying the $\boldsymbol{a}$ lattice parameter by $\sqrt{2}$. Using this lattice as the reference state for convenience, the fcc phase would be one having $\boldsymbol{a} \equiv \boldsymbol{c}$. Conversion of the fcc δ-hydride phase to the fct γ-hydride phase, then, involves a contraction in the $\boldsymbol{a}$ directions and an expansion in the $\boldsymbol{c}$ direction of the δ-hydride phase of magnitudes such that $\boldsymbol{c/a} > 1$. The reverse occurs for the conversion of the fcc δ-hydride phase to the fct ε-hydride phase, resulting in $\boldsymbol{c/a} < 1$. In this latter case, the increase in hydrogen composition of the ε-hydride

[1] It should be noted that Beck erred in describing the γ- and ε-hydride phases as having bct structures, which all other investigators have determined to have fct structures. However, this does not affect his arguments since Beck based his analysis on differences in the hydrogen composition in the transformation of the δ-hydride phase to an fct one having either positive or negative $\boldsymbol{c/a}$.

phase from its value at the $(\delta + \varepsilon)/\varepsilon$ phase boundary to its terminal, stoichiometric composition, ZrH_2, results in an increase in $\boldsymbol{a}$ and a corresponding decrease in $\boldsymbol{c}$, with the latter decreasing less than the increase in $\boldsymbol{a}$, thus resulting in a continuous reduction in $\boldsymbol{c/a}$ over the phase field composition, Fig. 2.1. As can be seen from this figure, this decrease flattens out as the stoichiometric composition of the hydride is approached and stops completely when this composition is reached and all the tetrahedral sites in this lattice are occupied by hydrogen atoms. Extrapolating this trend in the opposite direction for the γ-hydride phase, starting from the fcc δ-hydride phase, it is conceivable that the (notional) removal of a sufficiently large number of hydrogen atoms from this initially fcc lattice results in an fct γ-hydride lattice that is exactly the reverse of the ε-hydride phase, having an increase of the $\boldsymbol{c/a}$ ratio with (notional) decrease in hydrogen composition until a composition is reached at which the observed lattice parameters and the $\boldsymbol{c/a}$ ratio for this phase are obtained. Similar to the composition that stabilized the ε-hydride phase, the only unique solution for the composition that could stabilize the γ-hydride phase would seem to be a stoichiometric one, the most likely choice being ZrH_r, with $r = 1$, in which only alternate tetrahedral sites would be filled with hydrogen. This prediction for the stable composition of the γ-hydride phase is also a consequence of the postulate that, with decreasing temperature, it is the precipitation product (instead of the "equilibrium" α-Zr phase) of the decomposition of the δ-hydride phase and must have a lower hydrogen composition than that of the parent, δ-hydride phase. This, then, leads to the conclusion that the γ-hydride's terminal composition should be saturated in hydrogen, which, on the basis of symmetry considerations and the available tetrahedral sites, again leads to the prediction that the only composition possible for this phase is ZrH_r, with $r = 1$.

On the basis of the relative X-ray diffraction intensities obtained by Beck and of visual estimates of the volume fraction of γ-hydride precipitates observed in metallographic samples, the maximum amount of γ-hydride phase that can form under ordinary circumstances was estimated to be 30 or 40 %. Using the proposed model for γ-hydride formation and assuming on the basis of the foregoing reasoning that γ-hydride formation is stoichiometric, of composition ZrH_r, with $r = 1$, a shift in the composition of the δ-hydride phase from $r = 1.3$ at the eutectoid to 1.6 at room temperature would result in a maximum volume fraction of precipitated γ-hydride phase of 44 % if no α-Zr phase were formed. This prediction is in good agreement with Beck's corresponding estimate derived from a comparison between the relative X-ray diffraction intensities and also from the observed volume fraction of γ-hydride precipitates as described in the foregoing.

The foregoing proposed model for the formation of the γ-hydride phase also provides an explanation for the disagreement among various investigators at the time as to the location of the $(\alpha + \delta)/\delta$ phase boundary from the eutectoid to room temperature. In all samples containing an overall composition of less than $r = 1.3$, appreciable amounts of the α-Zr phase were observed. This is as expected since this phase would be formed as an equilibrium product of the eutectoid reaction. However, once the total amount of hydrogen in the sample exceeds this composition, the amount of α-Zr phase present would be insufficient for its detection by

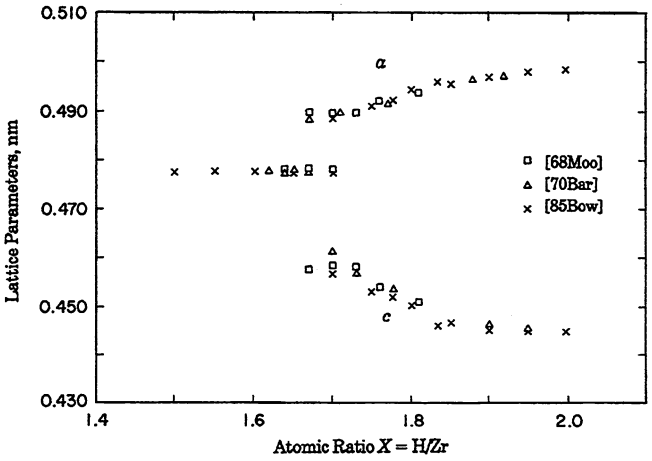

Fig. 2.1 Hydrogen composition dependence of Zr–H lattice parameters (from *left* to *right*) of the δ, $\delta + \varepsilon$, and ε phase regions at room temperature (from Zuzek et al. [34]). The symbols refer to the following sources: [68 Moo]—Moore and Young [20]; [70 Bar]—Barraclough and Beevers [5]; [85 Bow]—Bowman and Clark [9]

X-rays, as was observed. Therefore, without the proposed model for γ-hydride formation as a reaction product of the δ-hydride decomposition, it would appear from these observations that above this overall composition the $(\alpha + \delta)/\delta$ phase boundary would similarly be at $r \cong 1.3$ at room temperature. However, taking on board the foregoing proposal that the γ-hydride phase is a metastable product of the decomposition of the δ-hydride phase, the correct $(\alpha + \delta)/\delta$ composition can be located quite easily by factoring in the volume fraction and terminal hydrogen composition, $r = 1$ of the γ-hydride phase.

Following this insightful study by Beck [7], a series of bulk hydrogenated specimens in the composition range from $ZrH_{1.27}$ to $ZrH_{1.92}$ were prepared by Barraclough and Beevers [5] to determine their room temperature metallography, microhardness, and crystal structure properties. It is shown that the findings of these authors support those of Beck.

Barraclough and Beevers [5] found that for specimens having overall compositions of $ZrH_{1.47}$, $ZrH_{1.52}$, and $ZrH_{1.57}$, in addition to a strong signal indicating copious amounts of the δ-hydride phase, there were also weak signals attributed to the γ-hydride phase. Results from the powder pattern of $ZrH_{1.27}$ also provided evidence of the presence of both the γ- and δ-hydride phases plus a small amount of a third phase that was not identified, but likely was the α-Zr phase on the basis of the results by Sidhu et al. [24] and microhardness measurements of Barraclough and Beevers [5]. Supporting metallographic studies of specimens in the composition range $r = 1.47$–1.57 showed that the γ-hydride phase appeared as banded precipitates of lenticular shape embedded in the majority δ-hydride phase (Figs. 2.2 and 2.3). Quantitative metallography showed the volume fraction of γ-hydride precipitates

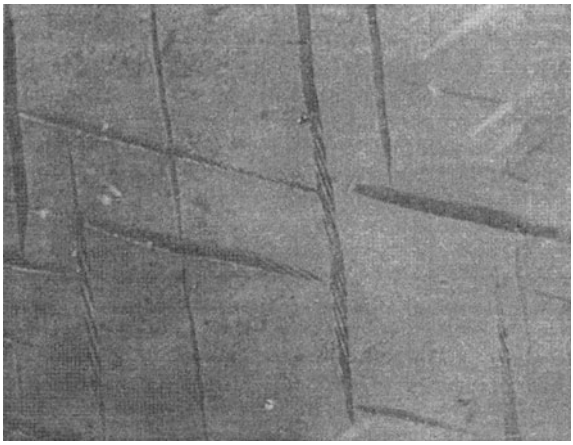

Fig. 2.2 Banded γ-hydride precipitates in δ-hydride matrix of $ZrH_{1.52}$ (from Barraclough and Beevers [5])

Fig. 2.3 The structure of a $ZrH_{1.27}$ specimen showing banded γ-hydride precipitates in a δ-hydride matrix and a third phase at the grain boundary (from Barraclough and Beevers [5])

increased as the overall hydrogen content decreased. Lenticular, γ-hydride precipitates within the δ-hydride matrix were also observed for the $ZrH_{1.27}$ specimens. The latter specimens showed some structural instability since re-examination of these specimens after 6 months revealed additional γ-hydride precipitates formed at the α–δ boundaries while small, globular precipitates of α-Zr were found at the δ grain boundaries. These findings are in agreement with Beck's proposed model for the decomposition of the δ-hydride phase at temperatures below the eutectoid and at overall hydrogen compositions ranging from, $r \cong 1.3$ to 1.6 . The metallographic evidence obtained by Barraclough and Beevers indicates that the γ-hydride phase forms in δ-hydride by a shear mechanism, with the banded structure indicating that this shear is relieved by alternate twinning of the lattice in opposite directions. A similar conclusion was formed for the formation of the ε-hydride phase in δ-hydride in the narrow composition range from $r \cong 1.6$ to 1.7 (Fig. 2.4). Beyond this composition all specimens contained only the ε-hydride phase, forming a completely

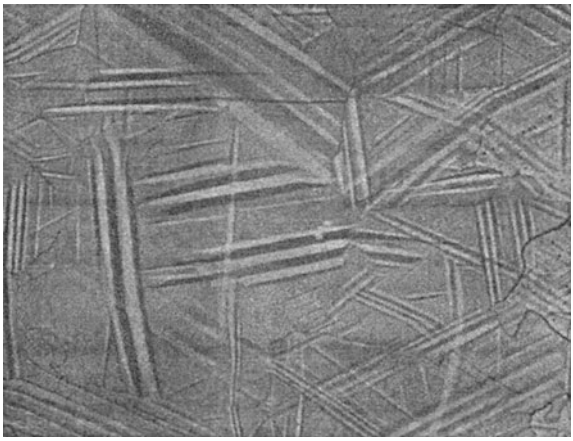

Fig. 2.4 The banded ε-hydride phase and untransformed regions of the δ-hydride phase in $ZrH_{1.71}$ (from Barraclough and Beevers [5])

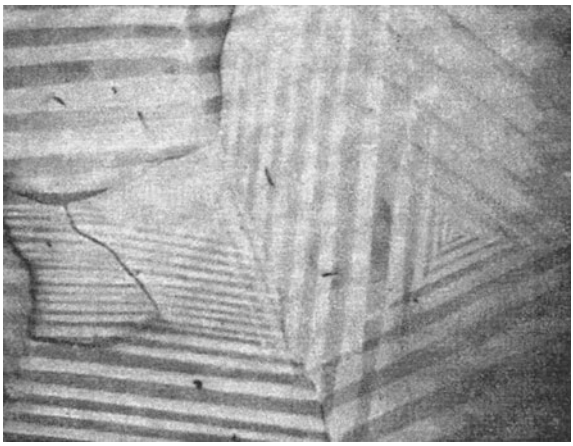

Fig. 2.5 The completely banded ε-hydride structure of $ZrH_{1.77}$ (from Barraclough and Beevers [5])

banded structure (Fig. 2.5). Barraclough and Beevers [5] found, in agreement with Beck [7], that in this phase field range the ***c*** lattice parameter and the ***c/a*** ratio of the ε-hydride phase decreased with increase in hydrogen composition while the ***a*** lattice parameter increased.

The suggestions by both Beck and Barraclough and Beevers that the formation of the γ- and ε-hydride phases in δ-hydride occurs essentially by a martensitic type transformation are supported by the analyses and experimental results of Cassidy and Wayman [10, 11] noting, however, that in contrast to a strictly diffusionless martensitic transformation these invariant plane strain transformations must be associated with a corresponding change in hydrogen composition. The need for a composition change creates some uncertainty in their analyses to determine the habit planes of the product γ- or ε-hydride precipitates of these transformations as it is not certain whether this occurs before, during or after the transformation.

Nevertheless, based on these observations, Barraclough and Beevers—taking on board the considerations of Beck regarding the nature of the δ- to ε-hydride phase transformation—suggest that the $(\delta + \varepsilon)$ phase field is actually not a true equilibrium one, but represents the range of compositions over which the martensitic transformation is stabilized as a result of factors such as the low jump frequency of the hydrogen atoms at room temperature and the creation of plastic deformation caused by the large transformation strains of the ε-hydride precipitates in the δ-hydride phase (the same considerations would apply to the γ-hydride phase). Barraclough and Beevers [5] note that the hydrogen jump frequency (Hon [15]) and dislocation mobility (Barraclough and Beevers [3]) are extremely temperature sensitive. Consequently, inhibition of growth of the ε-hydride phase, either by the low jump frequency of hydrogen or by irrecoverable plastic deformation in the δ-hydride matrix, would be expected to decrease as the martensitic start temperature is increased; i.e., as the hydrogen concentration increases, the transformation temperature range between start and finish of the martensitic transformation from δ- to ε-hydride would be expected to decrease. For the similar δ- to γ-hydride transformation there is only one composition over which this occurs, and thus there would be no variable composition range over which the transformation is stabilized. However, as with the δ- to ε-hydride transformation, the rate of conversion would obviously be a function of temperature, decreasing with decreasing temperature. Although the ε-hydride phase is generally not formed for hydrogen compositions in zirconium alloys of practical interest in nuclear applications, and is therefore not of direct interest for the topic of this book, the transformation characteristics of this phase and its parallelism with that of the γ-hydride phase provide useful insights into the behavior and prevalence of the latter phase. This is the reason for which the characteristics and the conditions leading to its formation have been presented here to the level of detail provided.

A more recent study of the phases present in bulk specimens of the Zr–H system was that of Simpson and Cann [25] who hydrogenated compact toughness specimens to hydrogen contents ranging from ZrH_0 to $ZrH_{1.6}$ to measure the fracture toughness of bulk zirconium hydride material over this composition range. Both commercial-grade, cold-rolled Zr and flattened Zr-2.5 Nb pressure tube material was used as starting material. The main difference between the two materials after hydrogenation was in the grain size (the unalloyed Zr material had smaller grain size) and in the morphology and distribution of the hydride phases. (The presence of the alloying element, Nb, in the starting pressure tube material appears not to have a significant effect on the properties of the bulk hydrides produced.) A feature of their hydrogenation procedure was that some of their specimens were hydrogenated at 600 °C and either furnace cooled or air quenched, while others were hydrogenated at 900 °C and furnace cooled (1 °C/minute).

For compositions below $r = 1$, the microstructures of the at 900 °C consisted of δ-hydride precipitates in an α-Zr matrix. In hydrogenated commercial grade Zr, the hydrides were very large and unconnected and contained γ-hydride needles, Fig. 2.6. The hydrogenated Zr-2.5 Nb specimens had large α-Zr grain sizes, but the hydrides were finely dispersed within these grains. Specimens hydrogenated

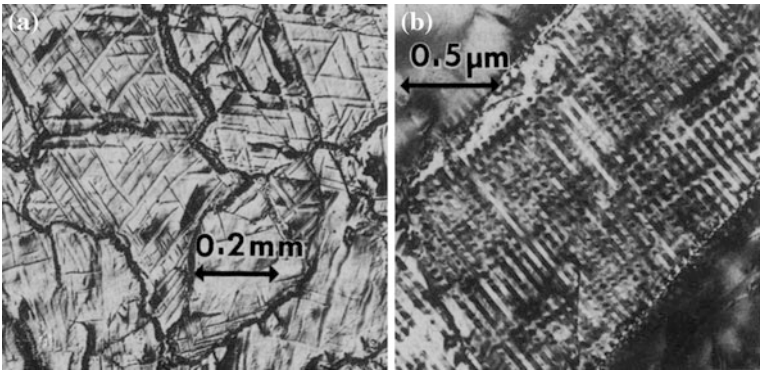

Fig. 2.6 Microstructure of $ZrH_{1.1}$: **a** Large δ-hydride grains containing γ-hydride needles; grain boundaries contain a mixture of α-Zr and unidentified hydride (bright field). **b** Transmission micrograph of γ-hydride needles, showing twinned structure (from Simpson and Cann [25])

at 600 °C (in the β or ($\beta + \delta$) region) had much finer grain sizes than those of the 900 °C series specimens. A $ZrH_{0.88}$ specimen was quenched from well within the ($\beta + \delta$) region and had a dispersion of α-Zr grains in a δ-hydride matrix. The $ZrH_{0.45}$ specimen, quenched from the β region, resulted in a fine grain structure with a grain boundary network of hydrides. The slow cooled specimen of composition $ZrH_{0.40}$ resulted in a similar structure, but on a considerably larger scale.

Compositions between $ZrH_{1.0}$ and $ZrH_{1.5}$ resulted in mixtures of δ- and γ-hydride phases, the proportion of the δ-hydride phase increasing with the hydrogen content. Some α-Zr phase was also observed at the low hydrogen content range of these compositions. The γ-hydride had formed as heavily twinned, needle-like precipitates, the twinning being revealed in TEM examinations. All specimens with hydrogen content greater than $ZrH_{1.5}$ consisted entirely of the δ-hydride phase.

It is evident that the types and proportions of phases observed in these hydrogenated fracture toughness specimens prepared by Simpson and Cann [25] were very similar to those obtained by previous workers such as Beck [7] and Barraclough and Beevers [5] for the same composition ranges. In general, all workers were able to produce crack-free hydrogenated specimens, although distortions were evident in specimens having plate or rectangular geometry. However, all of the workers also found that specimens in a narrow range from $r \cong 1.5$ to 1.66 either contained cracks or cracked during surface preparation, indicating exceptional brittleness for solid hydride specimens of that composition range, which is approximately the range over which the hydrogenated solid is made up solely of the δ-hydride phase.

2.1.3 Crystallography of the δ-Hydride Phase

The δ phase is a disordered fcc lattice of the CaF_2 prototype, space group (Fm 3m) with room temperature lattice parameter, $\boldsymbol{a_0} = 4.778$ Å [7]. This results in a unit cell volume, $\boldsymbol{a}^3$, of 109.07 Å. Similar to the γ phase, there are four Zr atoms in a unit cell of δ hydride. Therefore, the atomic or molar volume of δ-hydride, $\Omega_{Zr}^{\delta-hyd}$ or $\bar{V}_{Zr}^{\delta-hyd}$, is 27.27 $Å^3$/(atom Zr) or 16.42×10^{6} m^3/(mol Zr), respectively. According to the studies of Simpson and Cann [25] presented in the foregoing, the r ratio in this phase varies from $\sim$1.6–1.64 at room temperature to $\sim$1.31–1.7 at the eutectoid temperature of $\sim$550 °C. These phase boundary compositions differ slightly from those given by others [5, 7, 20] and others, as summarized by Zuzek et al. [34]. The lower numbers in each of the foregoing range intervals are those that apply at the $(\alpha + \delta)/\delta$ phase boundary. At this composition the entire two-phase material has been converted to the δ phase, above which there is a narrow range throughout which the δ-hydride phase increases in composition until the $\delta/(\delta + \varepsilon)$ phase boundary is reached. Although earlier results had found that the room temperature lattice parameter of the δ phase is approximately constant with hydrogen composition over the composition range, $r \cong 1.56$ to 1.70 (see Fig. 2.1 and the references cited therein) the results of Yamanaka et al. [31–33] show that there is a slight increase while the lattice parameter of ZrD_r over this composition range is slightly smaller than that of ZrH_r and has a weaker composition dependence. However, in addition to the composition dependence, because the concentration of hydrogen in the hydride at the $(\alpha + \delta)/\delta$ phase boundary varies with temperature, as shown in Fig. 2.7, so will the hydrogen molar volume. From Eq. 2.2 for $r = 1.5$, which is at the midpoint in the temperature variation of the H/Zr ratio, the molar volume of hydrogen in δ-hydride, $\bar{V}_H^{\delta-hyd}$, is 1.607×10^{-6} m^3/mol H. It is interesting to note that the molar volume of hydrogen in δ-hydride is approximately the same as that in γ-hydride for this hydrogen concentration even though a γ-hydride precipitate has a smaller volume expansion in α-Zr than does the δ-hydride precipitate. As is shown in Chap. 8, this demonstrates the importance of accounting for the hydrogen concentration, not only in the α-Zr phase, but also in the corresponding hydride phase in formulations of the chemical potential of hydrogen in α-Zr in local equilibrium at the $\alpha/(\alpha + \delta)$ and $(\alpha + \delta)/\delta$ phase boundaries.

Although it is evident from the foregoing that the molar volume of hydrogen in δ hydride varies with temperature because its hydrogen composition, r, varies with temperature, there would also be a variation in this molar volume (as well as in the other molar volumes and transformation strains from which the hydrogen molar volume is derived) with temperature and composition if the differences in the lattice parameters between the α-Zr and δ-hydride phases vary with temperature and composition. Recently, Singh et al. [26] evaluated the temperature and composition dependence of these differences using data provided by Douglass [12] for the temperature dependence of the lattice parameters in α-Zr and by Yamanaka et al. [31, 32] for the temperature dependence and hydrogen composition dependence of the lattice parameter in δ-hydride. Singh et al. [26] focused on the

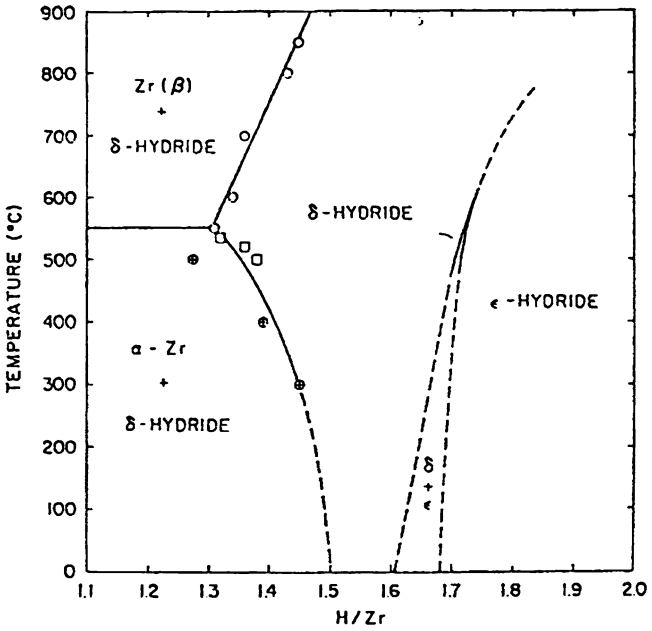

Fig. 2.7 The high hydrogen composition region of the Zr-H phase diagram (from Libowitz [18])

temperature dependence of the lattice parameters for a single δ-hydride phase composition of $r \cong 1.66$. Their results are reproduced in Fig. 2.8 showing that the variation with temperature of the difference in the lattice parameters of the two phases is not large. The largest difference in the temperature dependence is between the ***a*** lattice parameters, while the difference between the ***c*** and ***a*** lattice parameters of the α-Zr and δ-hydride phases, respectively, is very small. Fig. 2.9 plots the variations in volumetric transformation strain and corresponding plate normal transformation strain as a function of temperature in which the variation with temperature of the composition of the δ-hydride at the $(\alpha + \delta)/\delta$ phase boundary, using the data summarized by Beck [7], is also included. The latter is obtained by combining the linear dependence on hydrogen composition determined by Yamanaka et al. [31, 32] of the δ-hydride phase's lattice parameter with that of the corresponding average thermal expansion coefficient that was determined by them over the temperature range from 298 to 573 K. In this calculation, it was assumed that the dependence of the average thermal expansion coefficient on hydrogen composition in δ-hydride would apply outside the measured temperature range, up to 400 °C. This exercise results in the following lattice parameter (in Å) dependencies on temperature and δ-phase hydrogen or deuterium composition, r_H or r_D, respectively:

$$\mathbf{a}^{\alpha-\mathrm{Zr}} = 3.23118 + 1.6626 \times 10^{-5} \times [\mathrm{T(K)} - 298] \tag{2.3}$$

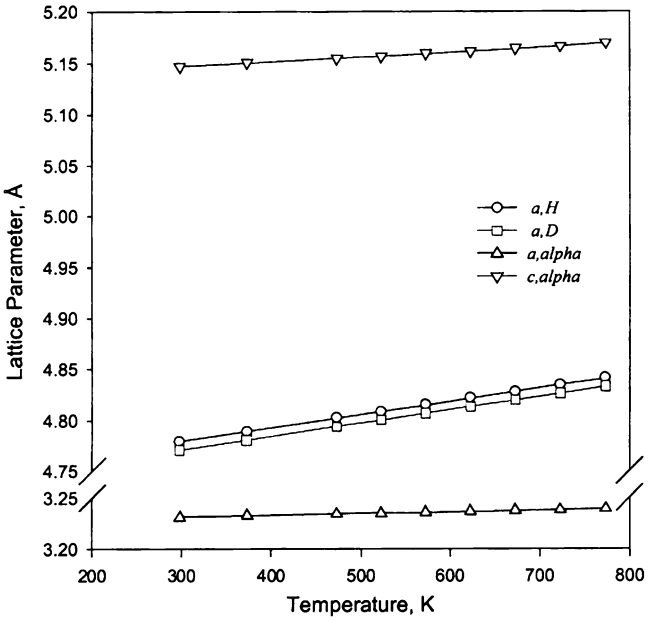

Fig. 2.8 Temperature dependence of the lattice parameters of hcp α-Zr, fcc δ-hydride $ZrH_{1.66}$ and fcc δ-hydride $ZrD_{1.66}$ (from Singh et al. [26])

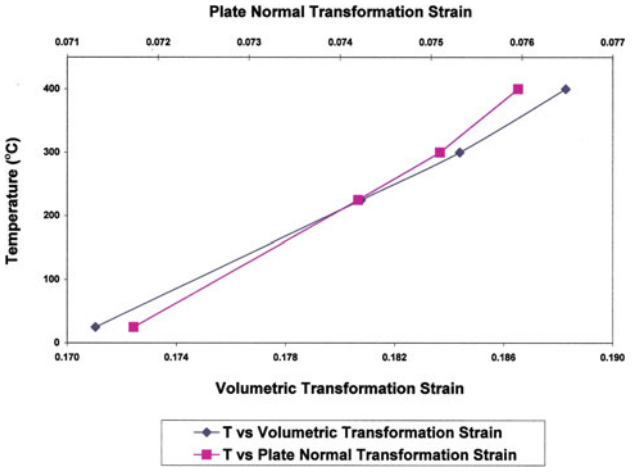

Fig. 2.9 Temperature dependence of plate normal transformation strain and volumetric transformation strain for δ-hydride at $(\alpha + \delta)/\delta$ phase boundary composition (the latter corresponding to chosen temperature based on Zr–H phase diagram of Beck [7])

$$\mathbf{c}^{\alpha-\mathrm{Zr}} = 5.14634 + 47.413 \times 10^{-6} \times [\mathrm{T(K)} - 298] \tag{2.4}$$

$$\mathbf{a}^{\delta-\mathrm{hyd(H)}} = 4.706 + 4.382 \times 10^{-2} \cdot \mathrm{r_H} + \left\{2.475 \times 10^{-5} + 6.282 \times 10^{-5} \cdot \mathrm{r_H} + 5.8281 \times 10^{-7} \cdot \mathrm{r_H^2}\right\}[\mathrm{T(K)} - 298] \tag{2.5}$$

$$\mathbf{a}^{\delta-\mathrm{hyd(D)}} = 4.738 + 1.961 \times 10^{-2} \cdot \mathrm{r_D} + \left\{2.492 \times 10^{-5} + 6.3119 \times 10^{-5} \cdot \mathrm{r_D} + 2.6081 \times 10^{-7} \cdot \mathrm{r_D^2}\right\}[\mathrm{T(K)} - 298] \tag{2.6}$$

Table 2.1 summarizes the temperature and composition dependencies of these and other key parameters of potential use for applications in mechanistic models of hydride and DHC behavior described in subsequent chapters.

The plot of Fig. 2.9 and the results summarized in Table 2.1 show that, in the temperature range of technological interest between room temperature and 400 °C, the increases in the dilatational transformation strains of δ-hydride are relatively small. However, for the molar volume of hydrogen in δ-hydride it can be seen from Eq. 2.2 that the explicit introduction of the hydrogen concentration, r_H, in the denominator results in a further variation in temperature dependence of the molar volume which is in the same direction as that of the lattice parameters, increasing its overall dependence on temperature in comparison to that of other parameters—such as the transformation volume and the individual dilatational transformation strain values—that depend only the lattice parameters' variations with temperature. The overall result is that the molar volume of hydrogen in the δ-hydride phase increases from 1.49×10^{-6} m^3/mol H at room temperature to 1.77×10^{-6} m^3/mol H at 300 °C, an increase of 0.28×10^{-6} m^3/mol H.

2.2 Mechanical Properties of Bulk Zirconium Hydrides

In this section, key results of elastic moduli, uniaxial deformation and fracture toughness parameters obtained from specimens of bulk zirconium hydride consisting of a single or a mixture of the α-Zr, γ-, and δ-hydride phases are presented.

2.2.1 Yield Strength

An early study by Beck and Mueller [8] of the tensile properties of bulk zirconium hydride specimens within the composition range $ZrH_{0.7}$ to $ZrH_{1.9}$ and the temperature range from room temperature to ~600 °C showed that macroscopic plastic deformation was not observed in the single phase δ– and ε-hydride composition ranges. Moreover, they were unable to produce crack free specimens in the hydrogen composition range $r = 1.53$–1.70, which is an indication of the

Table 2.1 Lattice Properties of δ-hydride at composition corresponding to the $(\alpha + \delta)/\delta$ phase boundary as a function of hydrogen composition. The values given are for the hydrogen isotope, protium (H), only

r_H	T (°C)	$a^{\alpha-\mathrm{Zr}}$ (Å)	$c^{\alpha-\mathrm{Zr}}$ (Å)	$a^{\delta-\mathrm{hyd}}$ (Å)	$\Omega_{\mathrm{Zr}}^{\alpha-\mathrm{Zr}}$ (Å^3/atom Zr)	$(\Omega_{\mathrm{Zr}}^{\delta-\mathrm{hyd(H)}})$ (Å^3/atom H)	$(\Omega_{\mathrm{Zr}}^{\delta-\mathrm{hyd(H)}} - \Omega_{\mathrm{Zr}}^{\alpha-\mathrm{Zr}})/r_H$ (Å^3/atom H)	$(\bar{V}_{\mathrm{Zr}}^{\delta-\mathrm{hyd(H)}} - \bar{V}_{\mathrm{Zr}}^{\alpha-\mathrm{Zr}})/r_H$ ($\times 10^{-6}$m^3 /mol H)	$(\Omega_{\mathrm{Zr}}^{\delta-\mathrm{hyd(H)}} - \Omega_{\mathrm{Zr}}^{\alpha-\mathrm{Zr}}/\Omega_{\mathrm{Zr}}^{\alpha-\mathrm{Zr}})$	$e_c^{\delta-\mathrm{hyd(H)}} = e_{33}^T$	$e_a^{\delta-\mathrm{hyd(H)}} = e_{11}^T = e_{22}^T$
1.61	25	3.2312	5.1463	4.7766	23.266	27.245	2.4715	1.488	0.1710	0.072	0.0453
1.5	225	3.2345	5.1552	4.7958	23.354	27.575	2.8144	1.695	0.1808	0.074	0.0484
1.47	300	3.2357	5.1586	4.8030	23.387	27.699	2.9335	1.767	0.1844	0.075	0.0496
1.42	400	3.2374	5.1635	4.8114	23.433	27.845	3.1070	1.871	0.1883	0.076	0.0509
1.37	454	3.2383	5.1664	4.8140	23.460	27.891	3.2348	1.948	0.1889	0.076	0.0512
1.33	504	3.2391	5.1693	4.8167	23.485	27.937	3.3473	2.016	0.1896	0.076	0.0515

extreme brittleness of such specimens in this composition range. Based on the phase diagram available at the time, the foregoing composition range is expected to produce specimens made up of only the single δ-hydride phase. The authors speculated that the extreme brittleness of their specimens was a consequence of a very low solubility in the δ-hydride phase of impurity elements present in the α-Zr starting material. According to Beck and Mueller [8], these impurity elements would be more soluble in the ε- than in the δ-hydride phase. As a result, these impurities would precipitate as small second phase particles in the δ-hydride phase and act as internal stress centers, making the bulk material consisting of this phase more susceptible to fracture during formation or grinding. This would, then, also explain why above $r = 1.70$ in the single phase ε-hydride composition region no difficulties were encountered with premature cracking of this material. Nevertheless, results of tensile tests of specimens consisting only of the ε-hydride phase always resulted in premature fracture at locations in the specimens other than the gauge region, indicating the extreme brittleness also of this phase, and making the testing of this material in tension highly sensitive to alignment problems.

The next attempt at determining the tensile properties of the δ- and ε-hydride phases was carried out by Barraclough and Beevers [3]. For tensile tests on specimens of overall composition, $ZrH_{1.66}$, they found that from room temperature to 500 °C fracture always preceded measurable plastic deformation. The stress at fracture was very low, in the range of approximately 48–69 MPa, with little dependence on test temperature. However, some of the specimens fractured outside of the gauge region. This was likely the result of non-axial loading that was a consequence of the warped shape of the hydrogenated specimens. As a result of these findings, all other tests were carried out in compression.

The results of the compression tests on specimens of composition $ZrH_{1.66}$ are reproduced in Fig. 2.10. Most of the tests were interrupted prior to fracture for examination of the specimens. Only those tests where this is indicated on the figure were taken to fracture. Below $\sim$100 °C these specimens were completely brittle, exhibiting no macroscopic plasticity. At temperatures from 100 to 120 °C, small plastic strains of $\sim$3 % could be accommodated prior to transgranular fracture. Metallographic examination of the polished surfaces of these fractured specimens revealed cracks and planar slip lines. Above 120 °C the intensity of slip markings increased and above 250 °C wavy slip lines was a predominant feature of the test results. Analysis of the slip lines on a specimen tested at 109 °C showed that the operative slip planes were of the {1 1 1} type. This type of slip was prevalent up to 250 °C, above which the slip lines became too wavy to be analyzed by the authors' microbeam X-ray and two-face stereographic analyses techniques.

Compressive tests of specimens with compositions $ZrH_{1.57}$, $ZrH_{1.52}$, and $ZrH_{1.47}$ were carried out between room temperature and 500 °C. These specimens consisted of the δ-hydride phase interspersed with an increasing volume fraction of γ-hydride platelets. A set of specimens with composition $ZrH_{1.27}$ were also tested over this temperature range. These specimens consisted of γ-hydride platelets in a predominantly δ-hydride matrix plus small amounts of α-Zr along the grain boundaries. All of these specimens were sufficiently ductile that they could be

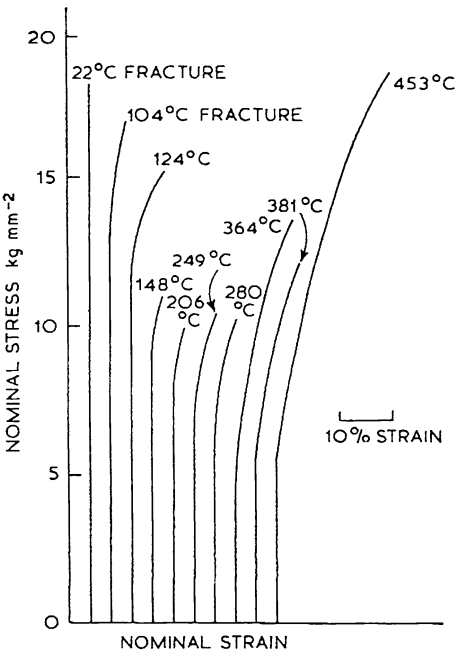

Fig. 2.10 Nominal stress–strain curves for the compressive deformation of $ZrH_{1.66}$ in the temperature range from 22 to 453 °C (from Barraclough and Beevers [3] ($10\,kg\,mm^2 \simeq 98\,MPa$))

taken beyond their limit of proportionality before fracture. The results of the dependence of the limit of proportionality on temperature, including the results from the tests on the $ZrH_{1.66}$ specimens, are plotted in Fig. 2.11. It is evident from this plot that the proportional limit in these specimens, consisting of two- or three-phase mixtures, decreases rapidly from its value at room temperature, leveling off, or reaching a local minimum, at about 200 °C. This means that above 150–200 °C, hydrides consisting of predominantly δ-hydride phase with an increasing proportion of γ-hydride platelets would deform plastically under compression at fairly low applied stresses. An important feature to note in the plot of Fig. 2.11 is the increase in proportional limit with temperature from 200 °C to a peak at 270 °C, beyond which it decreases again with further increases in temperature. The height of this peak increases with decrease in hydrogen content of the specimens. Based on the model developed by Beck [7] for why the volume fraction of the γ-hydride phase increases with decrease in overall hydrogen content, the peak likely reflects the changes in the deformation properties of the two-phase mixture brought about by the dissolution of the γ-hydride phase as the temperature is increased. Hence, this effect would be greatest for the specimens with the lowest total hydrogen content, for which the volume fraction of the γ-hydride phase would be largest. Supporting evidence for the dissolution of the γ-hydride precipitates and their subsequent re-precipitation upon cooling was obtained from room temperature metallographic examinations of specimens tested above 280 °C. These showed that the γ-hydride platelets tended to be much smaller and were undistorted,

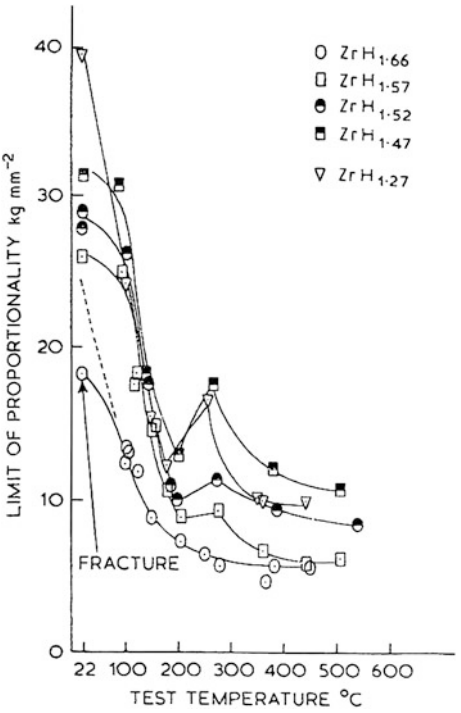

Fig. 2.11 Temperature dependence of the limit of proportionality of bulk hydride specimens consisting of δ-hydride, ($\delta + \gamma$)-hydride and ($\delta + \gamma + \alpha$)-hydride phases (from Barraclough and Beevers [3])

in contrast to the distorted γ-hydride platelets observed in the interior of sectioned specimens that had been tested at lower temperatures. However, a specimen of composition $ZrH_{1.27}$, tested at 360 °C, still showed the presence of large, distorted γ-hydride platelets, indicating that these precipitates had not been completely dissolved at that temperature.

To obtain information on the microscopic fracture process in the specimens exhibiting some ductility at room temperature prior to macroscopic fracture, a series of interrupted room temperature tests were carried out by Barraclough and Beevers on specimens of compositions $ZrH_{1.47}$ and $ZrH_{1.52}$. Surface cracks were first observed at 189 and 186 MPa, respectively. The cracks were initiated in the δ-hydride phase and not in the γ-hydride needles. In fact, there was evidence that these precipitates could sometimes act as crack arresters, Figs. 2.12 and 2.13 shows the evolution of surface cracks in a specimen of composition $ZrH_{1.47}$ which had a proportional limit of 311 MPa.

The Burgers vectors of the dislocations responsible for the observed slip on {1 1 1} planes were not experimentally determined by Barraclough and Beevers, but are expected to be of $\boldsymbol{a}/2 < 1\ 1\ 0 >$ types, based on the lattice structure of the δ-hydride phase (CaF_2) and results in the literature for ionic crystals with such structure. However, the predominant slip planes in ionic crystals are {1 0 0}. This suggests that the occurrence of slip on {1 1 1} planes is indicative of considerable metallic bonding. Assuming, then, that the slip systems in the δ-hydride phase are

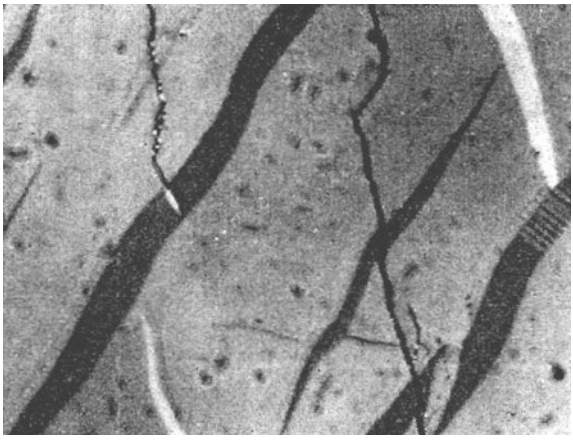

Fig. 2.12 The surface of a $ZrH_{1.52}$ specimen after 0.5 % strain at room temperature, showing a crack arrested in a γ-hydride platelet (from Barraclough and Beevers [3])

of $\{1\ 1\ 1\} < 1\ 1\ 0 >$ types, Barraclough and Beevers conjectured that the extreme brittleness of this phase could be the result of the influence of the hydrogen lattice on the movement of the Zr lattice glide dislocations. The authors suggest that it is the hydrogen vacancies (i.e., the unoccupied tetrahedral lattice sites in the CaF_2-type lattice) that act as the primary source of lattice friction for dislocation movement. This suggestion is supported by the sharp decrease in microhardness between $ZrH_{1.60}$ and $ZrH_{1.66}$ (reproduced further on) and the results given in Fig. 2.11 showing that from 400 to 500 °C—throughout which it is thought only the δ-hydride phase would be present—the limit of proportionality decreases with an increase in hydrogen content. The rapid decrease in proportional limit above 100 °C may then be the result of the reduction in influence of the hydrogen lattice because of the increased mobility of the hydrogen atoms in the δ-hydride phase. However, the influence of the vacant hydrogen lattice sites is nevertheless still evident in affecting its ductility, as evidenced by the low values of the limits of proportionality plotted in Fig. 2.11 in the temperature range from 300 to 400 °C. Over this temperature range, it is thought that the γ-hydride precipitates would have been dissolved and the specimens would have consisted only of δ-hydride phase (Fig. 2.11). Moreover, the limits of proportionality of the $ZrH_{1.57}$, $ZrH_{1.52}$, and $ZrH_{1.47}$ specimens, which decreased rapidly with temperature from 100 to 200 °C, were virtually independent of hydrogen content over this temperature range. This observation is consistent with the ($\delta + \gamma$) material having a δ-hydride matrix that would retain its low temperature composition of $\sim ZrH_{1.59}$ over this temperature range. Metallographic evidence showed that the limit of proportionality is primarily controlled by the deformation characteristics of the δ-hydride matrix which, in turn—based on the foregoing reasoning—would be controlled by the number of vacant hydrogen lattice sites. Therefore the limit of proportionality would remain independent of overall hydrogen content, as a result of the conjectured constancy of the composition of the δ-hydride phase in these ($\delta + \gamma$) alloys. Note also that the limits of proportionality of the ($\delta + \gamma$) materials were always

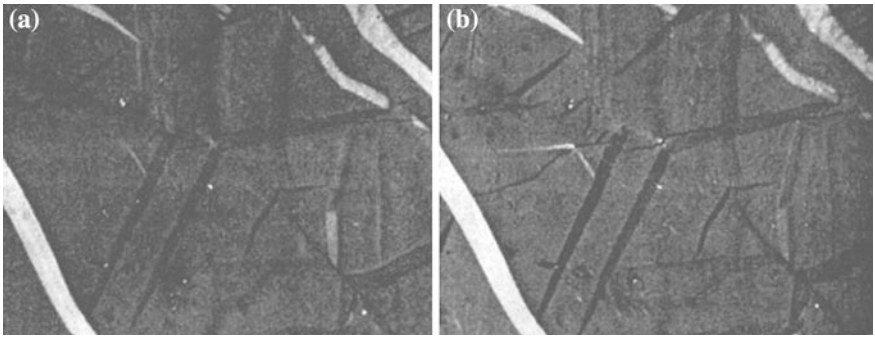

Fig. 2.13 Surface cracks on a $ZrH_{1.47}$ specimen loaded at room temperature to, **a** 189 MPa and, **b** 249 MPa (from Barraclough and Beevers [3])

greater at any given temperature than those of the single phase δ-hydride materials, which is also consistent with the foregoing conjecture concerning the role of hydrogen vacancies in controlling the mobility of dislocations. Further, the foregoing observation of distorted γ-hydride platelets in specimens containing $(\delta + \gamma)$ material shows that these precipitates would not have had significant influence on the yield characteristics over the temperature range from 100 to 200 °C.

Based on these considerations, the peak at $\sim$270 °C in the plots of Fig. 2.11 can be explained on the basis of the increasing dissolution of the γ-hydride phase. Support for this comes from the findings of Sidhu et al. [24] who reported that a transformation from $(\delta + \gamma)$ to $(\delta + \alpha)$ occurs at $\sim$250 °C and from Beck [7] who reported fast reaction kinetics for the dissolution of the γ-hydride phase. The dissolution of this phase results in an increased hydrogen vacancy concentration in the δ-hydride matrix since its overall hydrogen composition decreases. This is also consistent with the increase in the limit of proportionality from 200 to 270 °C being greater for materials with lower hydrogen content, which is expected if the vacancy concentration in the δ-hydride phase is responsible for controlling the deformation characteristics. Further support for Barraclough and Beever's conjecture that there is considerable dissolution of the γ-hydride phase above 200 °C came from the observations that the γ-hydride precipitates were not distorted in specimens tested above this temperature.

As seen in Fig. 2.11, the dependence of the proportional limit of the $ZrH_{1.27}$ specimens on temperature does not follow the trend with hydrogen composition observed for specimens with hydrogen contents, $r \cong 1.47$ to 1.57. However, the $ZrH_{1.27}$ specimens contained large, distorted γ-hydride platelets (Fig. 2.14)—even after testing at 360 °C—indicating that not all of the γ-hydride precipitates had been taken into solution. For such a case, the δ-hydride matrix would have a composition that is dependent on the reaction kinetics of the three-phase material, which would be expected to decrease from its low temperature value of $r \cong 1.59$ on partial dissolution of the γ-hydride precipitates, based on the two-phase composition of the $(\alpha + \delta)/\delta$ phase boundary shown in Fig. 2.7.

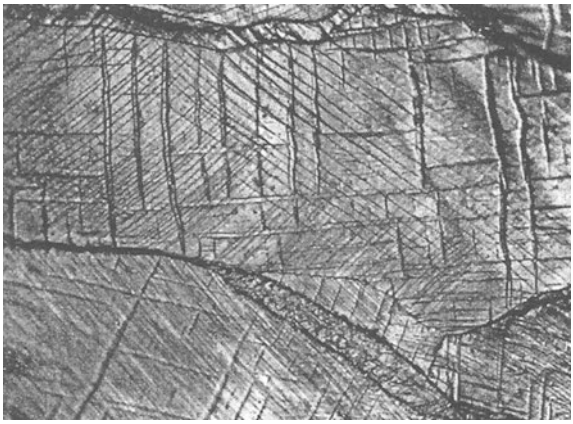

Fig. 2.14 Large distorted γ-hydride platelets in a $ZrH_{1.27}$ specimen after 11 % strain (from Barraclough and Beevers [3])

An attempt was made by Barraclough and Beevers [3, 4] to explain the fracture characteristics of the various materials. As noted, the specimens of composition $ZrH_{1.66}$ tested in tension were extremely brittle, in agreement with the results of Beck and Mueller [8]. Since the available $\{1\ 1\ 1\} < 1\ 1\ 0 >$ slip systems would satisfy the von Mises requirement for polycrystalline ductility, the observed brittle behavior must come from the increased lattice friction imposed on the dislocation mobility by the hydrogen vacancies in the δ-hydride matrix.

From the results of Fig. 2.15 it is seen that cracks are formed in the $ZrH_{1.66}$ and $ZrH_{1.59}$ specimens at approximately the same applied stress value. The influence of the volume fraction of the γ-hydride platelets is plotted in Fig. 2.16. From metallographic observations there was an increase in hydride precipitate size and interspacing. If these γ-hydride platelets were to act as crack nucleation centers, then the fracture stress would be expected to decrease with increase in volume fraction of this phase, which is contrary to observations (Fig. 2.16). The results in Fig. 2.15 show that cracks appeared in the specimens at applied stresses well below those for final fracture, indicating that the increase in fracture stress could be associated with the restrictions on crack growth as a result of the γ-hydride platelets as shown in Fig. 2.12. The γ-hydride platelets were observed to have $\{1\ 0\ 0\}$ habit planes in the δ-hydride matrix, which means that if the cleavage planes in both hydrides are the same—of $\{1\ 1\ 1\}$ type—then the cracks must change their directions to pass through the γ-hydride platelets. These precipitates also exhibited a twinned micro-structure that, by further twinning as a result of the increasing external stress, could possibly offer further resistance to crack propagation. These considerations lead to the conclusion that the primary role of the γ-hydride platelets during the deformation process was to inhibit crack propagation, rather than to act as crack nucleation centers. For the one set of specimens consisting of $(\delta + \gamma + \alpha)$ material ($ZrH_{1.27}$), the observation of a further increase in inhibition of crack propagation was probably the result of the additional presence of the more ductile α-Zr phase. Based on these considerations, it is likely that the deformation in region A-B in Fig. 2.15—throughout which micro-crack

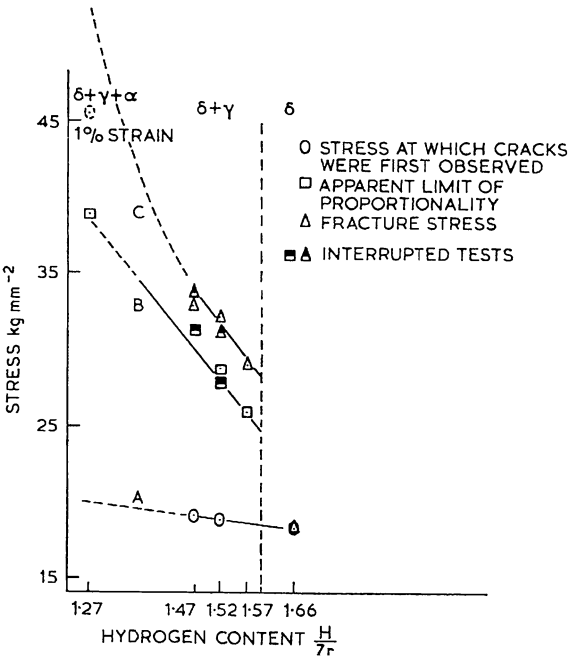

Fig. 2.15 The fracture and deformation characteristics of δ-hydride, $(\delta + \gamma)$-hydride and $(\delta + \gamma + \alpha)$-hydride phases (from Barraclough and Beevers [3])

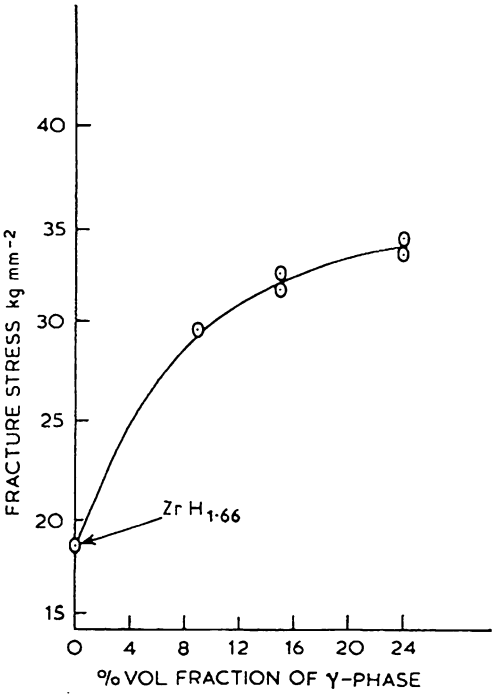

Fig. 2.16 Influence of volume fraction of second-phase γ-hydride platelets on the room temperature fracture stress of $(\delta + \gamma)$-hydride material (from Barraclough and Beevers [3])

nucleation and propagation occurred—may be mainly the result of shape changes in the specimen associated with this process.

Recently, Puls et al. [23] summarized results of additional compressive deformation tests on solid zirconium hydride specimens of hydrogen composition ranging from $ZrH_{1.0}$ to $ZrH_{1.9}$. Starting materials for these solid zirconium hydride specimens were either cold-worked Zr-2.5 Nb pressure tube or reactor grade unalloyed Zr material. In addition, two different hydrogenation temperatures, 850 or 600 °C, were used. The results obtained by Barraclough and Beevers [3, 4] have shown that specimens consisting of single phase δ-hydride exhibited no macroscopic plasticity prior to fracture below 100 °C while external cracks had formed at applied external stress values below the proportional limit for more ductile specimens such as those consisting of ($\delta + \gamma$)-hydride phases or of single phase δ-hydride material tested at temperatures above 100 °C. This extremely brittle behavior of the material tested by Barraclough and Beevers [3, 4] may have been exacerbated by the likely presence of microscopic cracks in the interior of the specimens produced during the hydrogenation process. These micro-cracks would have affected the deformation characteristics of the specimens. To obtain a truer measure of the deformation characteristics of solid zirconium hydrides, Puls et al. [23] carried out compression tests under a confining hydrostatic pressure, thereby hoping to mitigate the effects of possible pre-existing microscopic cracks formed during hydrogenation of the specimens on the material's deformation behavior.

The testing apparatus used for this purpose was a modified Griggs machine at the Laboratoire de Métallurgie Physique of the Université de Poitiers, France [29]. This machine allowed for separate control of the uniaxial compressive stress and a surrounding pressure that was applied by means of a solid confining medium. The first set of uniaxial compression tests was carried out under a confining pressure of 1,000 MPa. Confined compression tests with this pressure were carried out mainly at room temperature with a few tests done also at 150 and 200 °C. A lower confining pressure of 400 MPa was used in most of the remaining tests out of concern that the higher confining stress may have affected the accuracy of the results by creating sufficiently high levels of friction stresses to produce noticeable increases in the proportional limit. Tests carried out at 400 or 415 °C were not done under confinement because of the low value of the proportional limit at that temperature and the greater ductility of the material. Initially the Griggs set up was used with the confining piston made of carbide having the same diameter as the surrounding jacket. As a result of the friction generated by this confinement, the accuracy of the stress–strain measurement results markedly decreased with this set up when the yield strength was much below 500 MPa, which turned out to be the case for specimens deformed at and above 100 °C. Improvements were, therefore, made to the Griggs machine to handle lower yield strength values by using a piston made of tungsten carbide having a diameter that was less than the surrounding jacket, thus reducing the friction produced by the confinement. Finally, it became evident that above about 100 °C all specimens were sufficiently ductile that they could be readily deformed into the plastic range in the Griggs machine without confinement. In addition—likely as a result of improved control in producing

crack-free ZrH_r specimens over the entire range of hydrogen composition of interest—it was found that unconfined compressive deformation at room temperature also gave acceptable results. Therefore, the last sets of tests consisted of standard uniaxial compression tests done with an INSTRON 4002 mechanical testing machine at AECL's Whiteshell Laboratories in Pinawa, Manitoba, Canada.

The results of all the tests at various temperatures and hydrogen composition carried out in France are listed in Table 2.2. The tests with test numbers starting with 'I' were unconfined tests done in an Instron machine, while all others, designated by test numbers starting with 'G', were done with the Griggs machine using either 1,000 or 400 MPa confining pressure as indicated. Comparing test results for specimens with closely similar hydrogen compositions, these results show that yield strength values for specimens having 1,000 MPa confinement were always somewhat higher than those obtained with specimens having a confinement of 400 MPa. Since only a few specimens tested under different confining pressure had the same hydrogen composition, it is difficult to quantify the increase in yield strength as a result of the higher confining pressure, but it appears to be in the range from 50 to 100 MPa. The exception to these results is for specimens G163 and G145 for which the reverse was true. The difference in yield strength of these two specimens of nominally identical composition was quite large, viz., 182 MPa.

For the tests done under hydrostatic confinement, two types of stress–strain curves were obtained as shown in Fig. 2.17a and b. The first type shown in Fig. 2.17a, exhibited by specimens with $1.3 < r < 1.62$, had high yield strength values showing a fairly sharp transition between the elastic and the plastic deformation regimes and little subsequent work hardening. The second type (Fig. 2.17b), with lower yield strength values and compositions $r < 1.3$ and >1.62, had a more gradual transition between the elastic and the plastic regimes and strong work hardening. Deformation was generally stopped in these series of confined tests before any macroscopic fracture of the specimens. Yield strengths in all tests were determined as given by the proportional limit, similar to what was used by Barraclough and Beevers [3, 4].

The yield strength results are plotted as a function of temperature in Fig. 2.18. Included in this figure are results obtained by Barraclough and Beevers. In this plot, the yield strength data given in Table 2.2 for closely similar values of r were rounded to the nearest integer, and a corresponding average yield strength value applicable to this average value of r was determined. This figure shows that there is a sharp drop in yield strength from room temperature to 150 °C, with little change up to 400 °C after that. The figure shows that the yield strength values of Barraclough and Beevers are consistently and significantly lower than those of Puls et al. at all temperatures and hydrogen compositions. The results of Puls et al. show that the highest yield strength values are found just below a hydrogen composition of $r \sim 1.7$. There is a large drop (minimum) in yield strength value at $r \sim 1.7$ and a gradual rise beyond that. The results of Barraclough and Beevers [3, 4] at 400 °C, taken from their plots of their Figs. 2.3 and 2.13, respectively, give a decrease at a composition $r \sim 1.48$–1.52 that continues to a composition of $r \sim 1.78$. Beyond this composition range all the nominal stress–strain curves obtained by Barraclough

Table 2.2 Yield strength versus hydrogen composition, *r*, at different temperatures from [23]; with permission from AECL

Specimen No.	Composition, *r*	Yield strength (MPa)
Temperature = ambient		
G232	1.00	622#
G223	1.12	633#
G170	1.21	751#
G142	1.21	794#
G225	1.25	636#
G165	1.37	870*
G140	1.43	968
G167	1.48	893*
G226	1.57	721#*
G224	1.61	746#*
G166	1.62	817*
G141	1.66	990
G168	1.67	607
G163	1.69	685
G145	1.69	503
G144	1.81	715
G230	1.83	431#
G231	1.86	529#
G169	1.89	672
G164	1.95	629
Temperature = 150 °C		
G211	1.30	646
G212	1.94	348
Temperature = 200 °C		
G235	1.15	170#
G236	1.58	122#
G234	1.90	185#
Temperature = 400 °C		
I5	1.21	118#
I6	1.43	158
I4	1.61	191
I2	1.72	88
I7	1.96	110
Temperature = 410 °C		
I15	1.15	150
I12	1.40	174
I11	1.57	192
I14	1.69	202
I10	1.91	140

All samples were hydrogenated at 850 °C from original Zr-2.5 Nb pressure tube material, except where otherwise indicated. (Specimens having specimen numbers starting with 'G' were tested under a confining pressure of 400 MPa; those bolded were tested under a confining pressure of 1,000 MPa. All other specimens were tested without confinement.)

Made from reactor grade Zr

*Hydrogenated at 600 °C

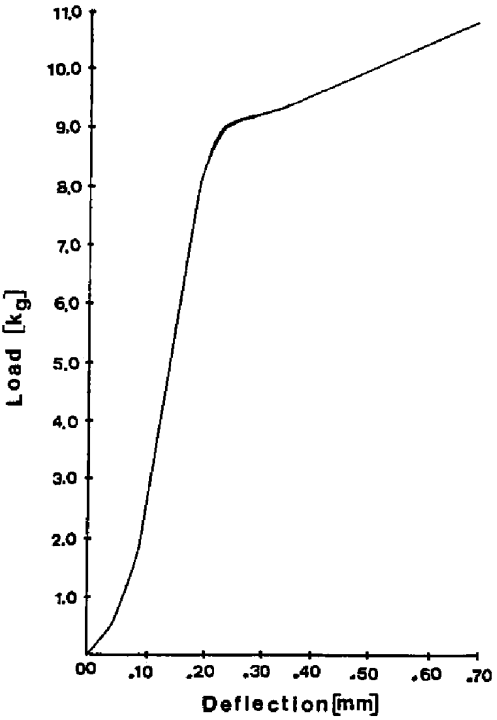

Fig. 2.17 **a** One type of load–deflection curve for ZrH_r hydride specimens with hydrogen composition, $1.3 < r < 1.62$ and deformed under confinement in the Griggs machine showing a fairly sharp transition between the elastic and plastic deformation regimes and little subsequent work hardening. (Specimen G167, $r = 1.48$; the vertical axis has been divided by 100) (from [23]). **b** One type of load–deflection curve for ZrH_r hydride specimens with hydrogen compositions $r < 1.3$ and $r > 1.62$ and deformed under confinement in the Griggs machine showing a gradual transition between the elastic and plastic deformation regimes and strong work hardening. (Specimen G168, $r = 1.68$; the vertical axis has been divided by 100) (from Puls et al. [23]; with permission from AECL)

and Beevers [4] exhibited load drops and, therefore, reliable yield strength values could not be obtained from these data. Puls et al. proposed that differences in the hydrogen composition dependences of the yield strength values obtained from the two sets of workers may be the result of the averaging procedure used by them in combining data obtained on material having slightly different compositions. The higher yield strength values and greater ductility, particularly at room temperature, obtained by Puls et al. are thought to be the result of their material containing fewer as-grown micro-cracks and/or the use of a confining pressure. For both sets of results, the lower yield strength values obtained at all temperatures for material containing only the ε-hydride phase may be partially the result of the greater number of flaws produced in forming materials having hydrogen contents close to those of the terminal composition of ZrH_2. The production of such flaws produced during hydrogenation is evident in Fig. 2.19 for a specimen of composition $ZrH_{1.8}$

Fig. 2.17 continued

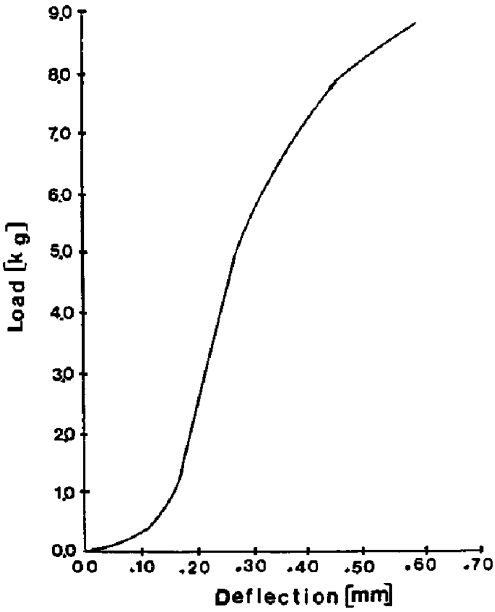

showing similar flaws both in the indentation region and outside of it. Thus, the "yielding" of the specimen may be the result of the (initially) stable growth of these flaws rather than being solely the result of the reduction in the onset of plastic deformation with temperature.

A set of cumulative deformations starting at $\sim$400 °C and decreasing in steps to room temperature were carried out for specimens of different hydrogen compositions. These results are plotted in Fig. 2.20. Such an experimental approach has the advantage that there are no differences (or uncertainties) in the hydrogen compositions of the specimens tested at different temperatures. The results are qualitatively similar to those of Fig. 2.18. However, the reduction in yield strength with temperature is greater for the non-cumulative tests. This may be connected with an annealing effect in the cumulative tests that was produced by each immediately preceding test, which was at a higher temperature. The yield strength values for the cumulative test at $r \sim 1.77$ stands out, being much smaller than those with hydrogen composition values greater and less than 1.77. This dip in yield strength over the complete temperature range tested is not evident in the non-cumulative tests (Fig. 2.18), perhaps because the relevant hydrogen composition was not part of the latter set.

A final set of room temperature deformation tests, but with no confinement, were carried out using an Instron machine. All specimens were deformed to failure, with the specimens broken into small pieces, indicating the extreme brittleness of this material at room temperature. The specimens with higher hydrogen compositions showed some ductility, but were still very brittle compared to non-hydrogenated, as-received material. Fig. 2.21 shows how the stress–strain

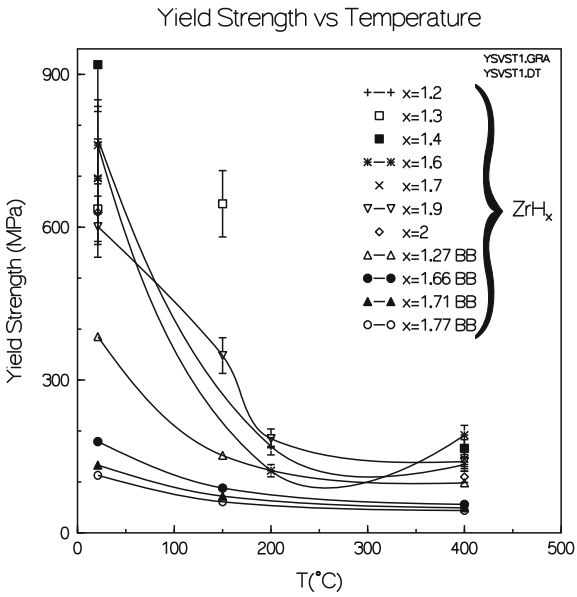

Fig. 2.18 Yield strength versus temperature for ZrH_r hydride specimens of different hydrogen compositions, $x \equiv r$. In the legend, BB refers to results obtained by Barraclough and Beevers [3, 4]. A spline fit was used to connect the points when data for three or more temperatures at a given $x \equiv r$ were available (from Puls et al. [23]; with permission from AECL)

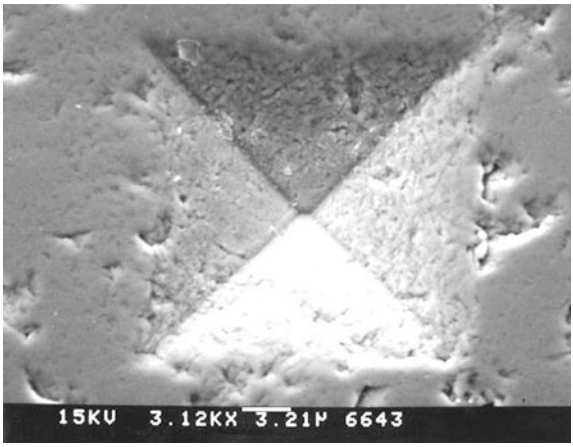

Fig. 2.19 SEM image of a micro-indentation on a specimen of $ZrH_{1.8}$ (from Puls et al. [23]; with permission from AECL)

behavior varied with r. The deformation curves obtained show a similar trend with r as those obtained under confinement; i.e., the curves for compositions $r = 1.4$–1.6 have higher yield strength values and sharper transitions to plasticity with only a limited work hardening stage beyond yield. However, the room temperature yield strength values derived from these unconfined tests are significantly lower compared to those obtained for corresponding compositions under confinement (Table 2.2). Figure 2.22 shows the room temperature variation of the yield strength with r. An abrupt drop in the yield strength with r is observed, starting from a composition for which—on the basis of the phase diagram—the

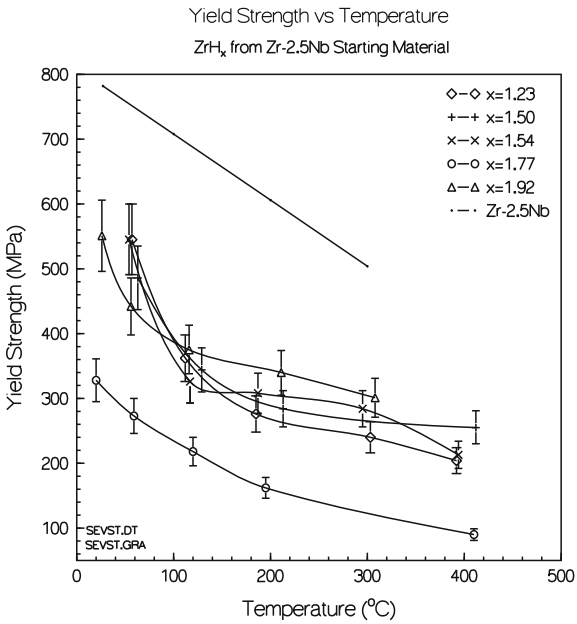

Fig. 2.20 Yield strength versus temperature obtained by cumulative deformation of each sample with a given hydrogen composition, $x \equiv r$, starting at the highest temperature. The solid line for Zr-2.5 Nb is the mean value for the temperature dependence of unirradiated, cold-worked Zr-2.5 Nb pressure tube material deformed in the transverse pressure tube direction (from Puls et al. [23]; with permission from AECL)

specimen is expected to consist only of the δ-hydride phase and reaching a minimum level at compositions at which the specimen is expected to contain only the ε-hydride phase. For both sets of results it is evident that the most brittle behavior is exhibited at compositions where δ-hydride is the dominant, or only, phase (from about $r \sim 1.5$–1.64). The brittleness of specimens with these compositions is further illustrated by the observation that, of five specimens tested with $r = 1.5$, three failed prior to reaching the plastic stage and all of the tests had small load drops in the elastic stage. The deformation curves for the specimens with compositions in the single phase ε-hydride range ($r \simeq 1.7$ and higher) are interesting, showing a two-stage plastic deformation stage not evident in the corresponding tests carried out under confinement. The reason for this difference in observation is likely because the latter tests were terminated prior to reaching the second work hardening stage.

2.2.2 Fracture Toughness

Simpson and Cann [25] carried out fracture toughness tests using miniature compact toughness specimens hydrogenated to hydrogen contents, ZrH_r, ranging from $r = 0$ to 1.64. Miniature specimens of 17 mm width were used to facilitate hydrogenation, but this posed problems in obtaining valid test results for specimens of low hydrogen content and/or tested at high temperature. Previous investigations had shown that tensile testing of material that had been

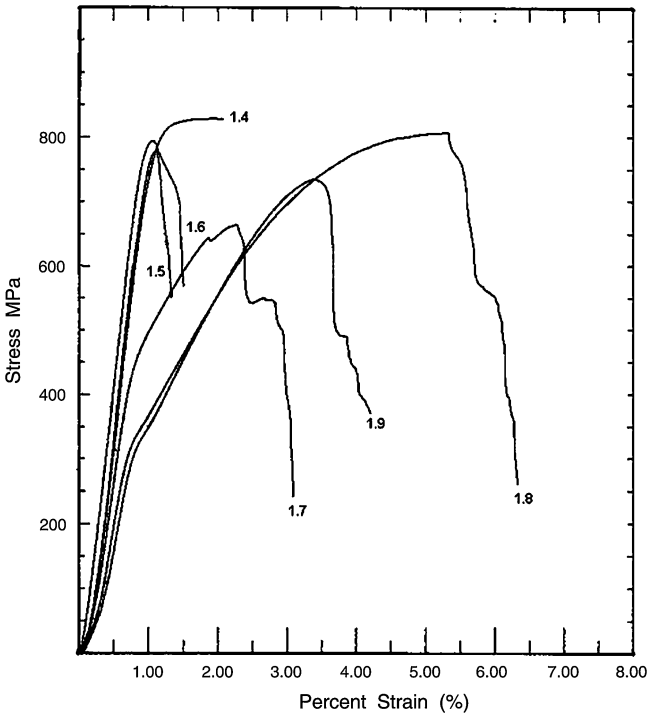

Fig. 2.21 Examples of stress–strain curves from room temperature unconfined deformation tests of ZrH_r hydride specimens. The numbers indicate the hydrogen composition, r (from Puls et al. [23]; with permission from AECL)

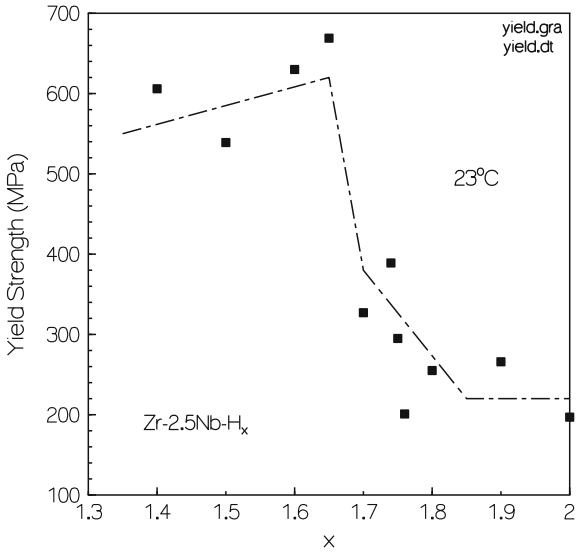

Fig. 2.22 Yield strength versus $x \equiv r$ of hydride specimens ZrH_r at room temperature from unconfined compression tests. The dashed line has been drawn to indicate the trend in the results (from Puls et al. [23]; with permission from AECL)

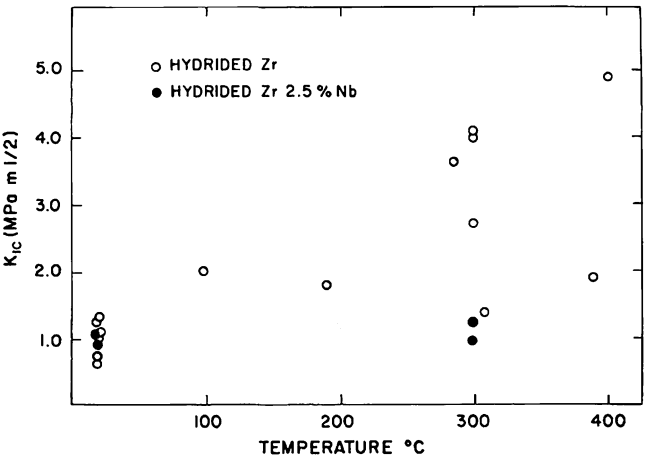

Fig. 2.23 Temperature dependence of K_{Ic} for ZrH_r in the composition range $r = 1.5$–1.64. Only the δ-hydride phase was identified to exist in these specimens (from Simpson and Cann [25]; with permission from AECL)

hydrogenated to a hydrogen composition where the specimen consisted mostly or entirely of the δ-hydride phase exhibited extreme brittle behavior, one reason for this behavior likely being that the hydrogenation process had resulted in the formation of many micro-cracks in the specimen. Thus, great care had to be taken to ensure the production of crack-free specimens. This turned out to be easier with reactor-grade Zr as the starting material compared to with Zr-2.5 Nb pressure tube material. Simpson and Cann [25] note that for specimens of hydrogen content, $r \geq 1.5$, only four successful tests could be carried out because of the difficulty in producing crack-free specimens from the latter starting material. The results of the dependence of fracture toughness, K_{Ic}, versus temperature are reproduced in Fig. 2.23. There is a large amount of scatter in the results, as one might expect given the low room temperature toughness of the material of only ~ 1 MPa$\sqrt{\text{m}}$. There is, however, clear indication from the upper bound values that fracture toughness increases significantly (relative to its room temperature value) within the interval from 200 to 300 °C. This is in contrast to the lower-bound toughness values showing no increase at all with temperature at this hydrogen content. The variation of K_{Ic} with hydrogen content, r, is reproduced in Figs. 2.24 and 2.25. These figures show that K_{Ic} increases gradually with decrease in hydrogen content down to $ZrH_{0.4}$ at which point it has a value of 10–15 MPa$\sqrt{\text{m}}$. The toughness values from the Zr-2.5 Nb pressure tube material yielded consistently lower results. Below a composition of $r = 0.4$ valid test results were difficult to obtain because of the increased ductility of the material combined with the small size of the compact toughness specimens. This was also true for some of the test results at 300 °C at $r = 0.4$. The K_{Ic} values calculated from the load–deflection data for these specimens are shown with a stroke through the open circle in Fig. 2.24 to indicate that they are "non-valid" test results.

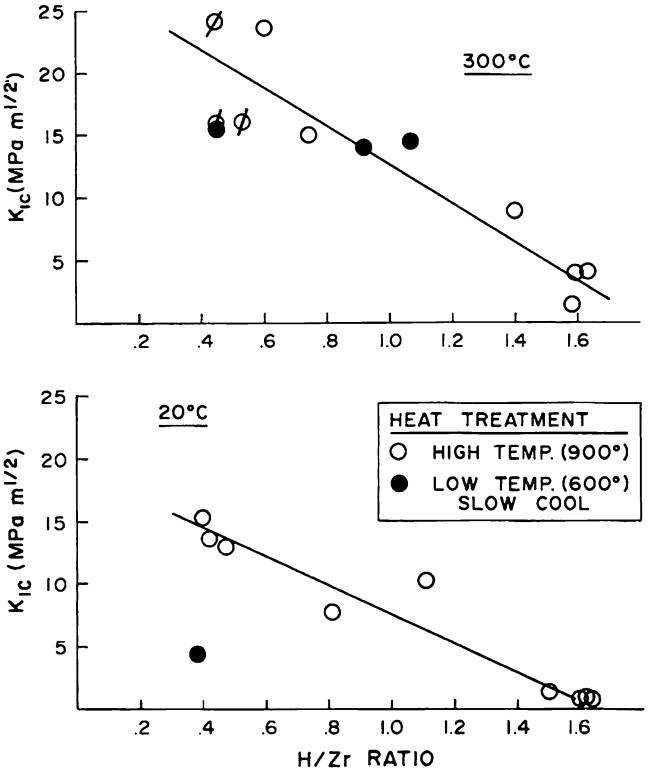

Fig. 2.24 Effect of hydrogen content on K_{Ic} of hydrogenated commercial-grade, cold-rolled zirconium starting material (from Simpson and Cann [25]; with permission from AECL)

2.2.3 Microhardness, Elastic Moduli, Internal Friction

Microhardness measurements provide a measure of the elastic and plastic response of a material over a relatively small area by determining the force required with an indenter to produce an indentation of a certain depth and size in the material. The virtue of these techniques is that it is relatively easy to use and does not require large specimen sizes. From these indentations, relationships have also been developed to determine parameters such the elastic modulus, yield strength, and some measure of fracture toughness of the material. The greatest utility of the microhardness results lies, however, in the observation that abrupt changes in their values seem to correlate with changes in the phase or phases present in the specimen, thereby providing another method of phase boundary composition determinations that could, moreover, be used on a micro or nano scale on embedded hydride clusters.

Among the earliest microhardness measurements on solid hydride specimens were those of Beck [7], Ambler [1] and Barraclough and Beevers [5]. Other

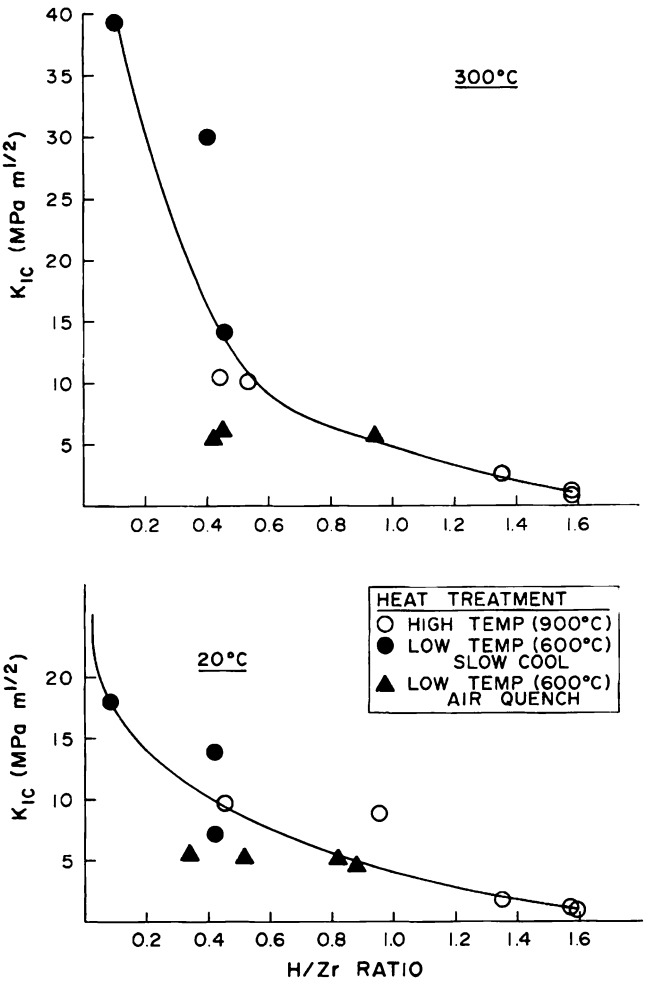

Fig. 2.25 Effect of hydrogen content on K_{Ic} of hydrogenated Zr-2.5 Nb pressure tube starting material (from Simpson and Cann [25]; with permission from AECL)

microhardness measurements were carried out by Syasin et al. [27], Yamanaka et al. [31–33], Xu and Shi [30] and Puls et al. [23]. In addition, all of these authors determined the elastic moduli of the hydrides studied, either through microhardness measurement techniques [23, 30] or using other methods, such as sound velocity [27, 31–33] and resonant oscillator technique [22]. The latter two sets of authors also measured the internal friction of the solid hydride specimens. The following account describes and assesses these results starting with the most recently published ones.

Using a composite oscillator technique running at 40 or 120 kHz, Pan and Puls [22] carried out simultaneous measurements of dynamic elastic modulus, *E*, and

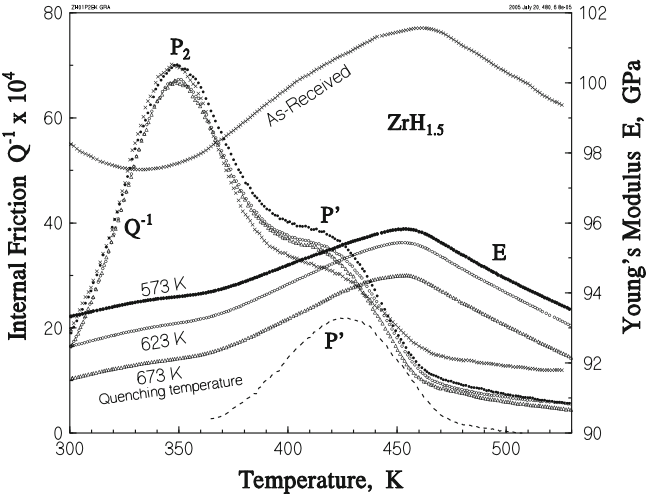

Fig. 2.26 Internal friction peak, P_2, a shoulder peak, P', and elastic modulus, E, in a $ZrH_{1.5}$ hydride specimen (from Pan and Puls [22]; with permission from AECL)

internal friction, Q^{-1}, as a function of temperature from room temperature to 300 °C for hydrogenated material of a single composition, $ZrH_{1.5}$. Two different source materials were used for the $ZrH_{1.5}$ specimens: reactor-grade, unalloyed Zr and Zr-2.5 Nb pressure tube material. After hydrogenation at 520 °C the specimens were annealed for 10 days at 400 °C and slowly cooled to room temperature. As-received (i.e., non-quenched) specimens and specimens quenched into cold water after a one hour anneal at 400, 350, and 300 °C, respectively, were tested. As seen in Figs. 2.26 and 2.27, the quenching treatment significantly decreased E at all temperatures from its values for as-received specimens. In addition, the different starting materials resulted in hydrogenated $ZrH_{1.5}$ specimens having significantly different temperature dependencies. E in the specimens hydrogenated from reactor-grade Zr material increased in value from room temperature to a peak at $\sim$180 °C, approximately independent of the quenching temperature while E obtained in the specimens prepared from Zr-2.5 Nb starting material had plateaux ranging from just above room temperature to 67 °C for the two quenched specimens and to 107 °C for the as-received specimen. Above these temperatures E decreased monotonically with increase in temperature. It is difficult to know the reasons for these differences. A possible cause may be the presence of $\sim$20 % volume fraction of γ-hydride platelets that was predicted by Beck [7] and Barraclough and Beevers [5] to be present at room temperature in the δ-hydride phase for material with this total hydrogen content. One might expect that, since the lattice structure of the γ-hydride phase is not cubic that it would have anisotropic elastic properties. Hence, differences in the lattice orientations, number, size, and internal microstructures (as a result of different amounts, types and orientations of twins) of these γ-hydride platelets as a result of differences in

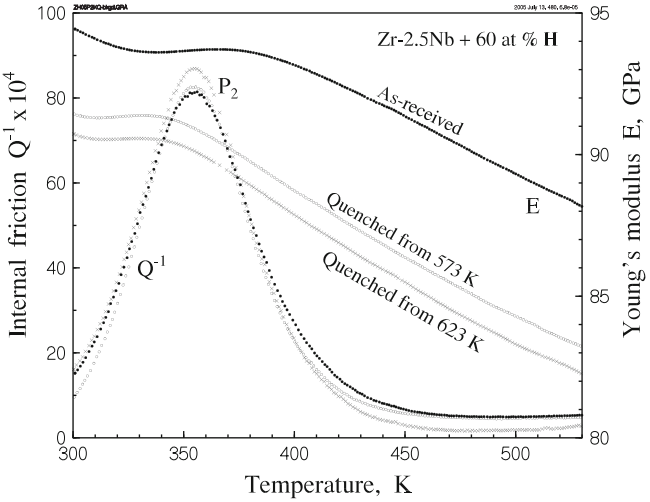

Fig. 2.27 Internal friction peak, P_2, and elastic modulus, E, in a Zr-2.5 Nb + 60 at % H (equivalent to $ZrH_{1.5}$) (from Pan and Puls [22]; with permission from AECL)

starting materials and heat treatments of the hydrogenated materials may then have resulted in differences in the average elastic properties. For $ZrH_{1.5}$ obtained from reactor-grade zirconium starting material, the room temperature value of E ranged from 98.2 to 91.6 GPa for the as-received material and for the material quenched at 300 °C, respectively, while for $ZrH_{1.5}$, derived from Zr-2.5 Nb pressure tube material, E ranged from 94.3 to 90.6 GPa for the as-received material and the material quenched at 250 °C, respectively.

Although there were differences as a result of the quenching treatment and source material for E, there was no difference in the peak temperature of the internal friction peak, P_2, and only small differences as a result of the foregoing factors. The interpretation proposed by the authors that the peak is the result of stress-induced jumps of hydrogen atom pairs in the δ-hydride phase, seems, at first glance, to be strongly supported by the finding that the amplitude of the peak depends on the square of the hydrogen content of the specimen ranging from very low hydrogen content to very high hydrogen content of $ZrH_{1.5}$ (60 at%). Such dependence would not be obtained if the origin of the P_2 peak were actually the result of a similar stress-induced jump process occurring in the $\sim$20 % volume fraction of γ-hydride phase predicted to be present at room temperature. This model would predict that the amplitude dependence of P_2 depends on the amount of hydrogen contained only in the γ-hydride phase. Moreover, it would predict that this dependence would be linear in this hydrogen concentration, since an internal friction peak as a result of a stress-induced jump process involving only a single hydrogen atom would be possible in the γ-hydride phase because of its non-cubic lattice structure.

Puls et al. [23] used a FISCHET H100 microhardness tester capable of evaluating the apparent elastic modulus $E' = E/(1 - \nu)$ below 55 °C using a diamond indenter

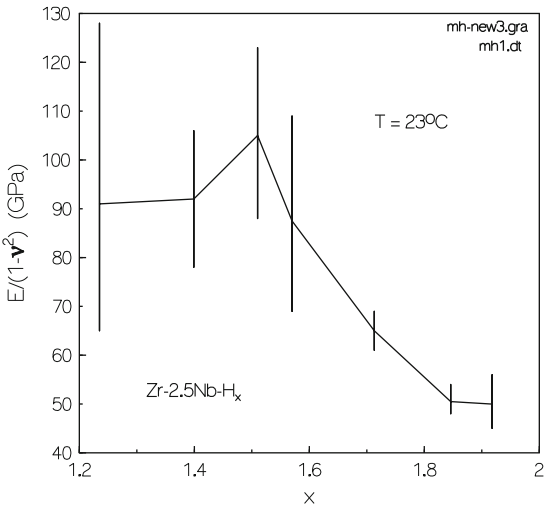

Fig. 2.28 Apparent elastic modulus of ZrH_x versus $x \equiv r$ at room temperature from microhardness tests using a diamond indenter (from Puls et al. [23]; with permission from AECL)

to measure the room temperature variation of E' as a function of the hydrogen content, r, on specimens similar to those that were used in their compression tests. The results are reproduced in Fig. 2.28 showing that there is a steep reduction in E' with increasing r starting at $r \sim 1.5$–1.6. Similar measurements were also made with the same equipment on the same type of specimens at elevated temperatures by replacing the diamond indenter with a sapphire one. Since the computer program supplied by the manufacturer for data acquisition and data analysis of the microhardness tester was calibrated for the low-temperature diamond indenter material only, the values of E' obtained are mainly useful in showing the relative variation of this parameter with temperature and composition. Fig. 2.29 gives three examples. It can be seen from this figure that E' decreases with increase in temperature and that the effect of increased hydrogen content is to shift the lines of E' to lower levels, while the rate of change with temperature for all of them is about the same as that of the original zirconium alloy.

Puls et al. [23] also determined the elastic modulus, E, directly from load–displacement plots of compression tests such as those shown in Fig. 2.21 based on the steepest linear portion of each load–displacement curve. The mean values are plotted in Fig. 2.30. The overall appearance of the E versus r plot is qualitatively consistent with what was obtained for the apparent modulus, E', from the microhardness test results (Fig. 2.28). There is a significant drop in E in the range from $ZrH_{1.6}$ to $ZrH_{1.8}$. This drop in microhardness with composition is echoed by a similar drop in the yield strength (Fig. 2.22).

Xu and Shi [30] used a nano-indentation technique for hardness measurements from which they derived values of elastic modulus and yield strength while the fracture toughness was determined using a microhardness indenter. Only bulk hydrogenated material of a single composition, $ZrH_{1.83}$, consisting mostly of the single ε-hydride phase, was investigated. An optical micrograph of the material

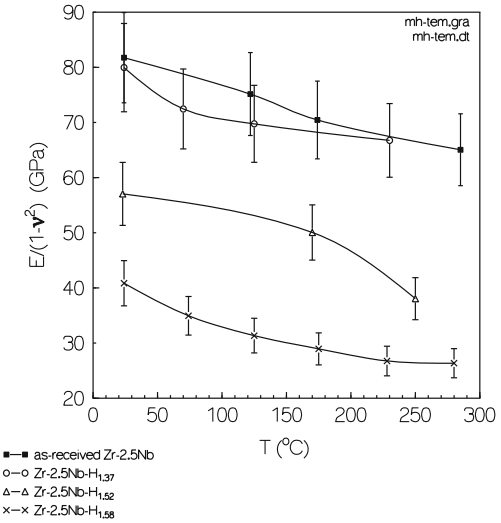

Fig. 2.29 Apparent elastic modulus of $ZrH_{1.37}$, $ZrH_{1.52}$, and $ZrH_{1.58}$ at elevated temperatures from microhardness tests using a sapphire indenter. A spline fit was used to connect the data (from Puls et al. [23]; with permission from AECL)

showed that the material contained voids, particularly along the grain boundaries. The presence of such flaws is consistent with metallographic observations of such flaws in most other hydrogenated specimens consisting only of the ε-hydride phase. The advantage of the nano-indentation technique, then, for such material is that the indentations are small enough that locations containing void-like defects could be avoided thus resulting in a truer picture of the intrinsic mechanical properties of the material. The authors obtained an average room temperature hardness value of 3.31 GPa for this composition, a yield strength of 478 MPa (compared to a yield strength of 780 MPa for the reactor grade zirconium starter material) and a reduced elastic modulus value of 67.66 GPa, derived from these hardness values. The relationship between the reduced modulus, E_r, and the true elastic modulus, E, of the material is given by

$$\frac{1}{E_r} = \frac{1-v^2}{E} + \frac{1-v_i^2}{E_i} \tag{2.7}$$

With the elastic modulus and Poisson's ratio of the indenter, E_i and v_i, given by 1140 GPa and 0.07, respectively, and arbitrarily using a value of 0.3 for v since a measured value at this hydride composition is not available for this parameter, E of hydride of composition $ZrH_{1.83}$ was calculated to be 65.44 GPa. (Note that Yamanaka et al. [31] obtain a value for v of 0.32, which is constant over a hydrogen composition range from $r = 1.5$ to 1.7.) This result compares with a value of 54.95 GPa for $ZrH_{1.83}$ derived from the results of E' determined by Puls et al. using the same value of v and of 37.5 GPa obtained by the former authors directly from the load–displacement curves of their uniaxial compression tests. In comparison, E determined for the zirconium reactor-grade starting material determined by Xu and Shi, assuming a value of 0.43 for v, is 80.90 GPa compared

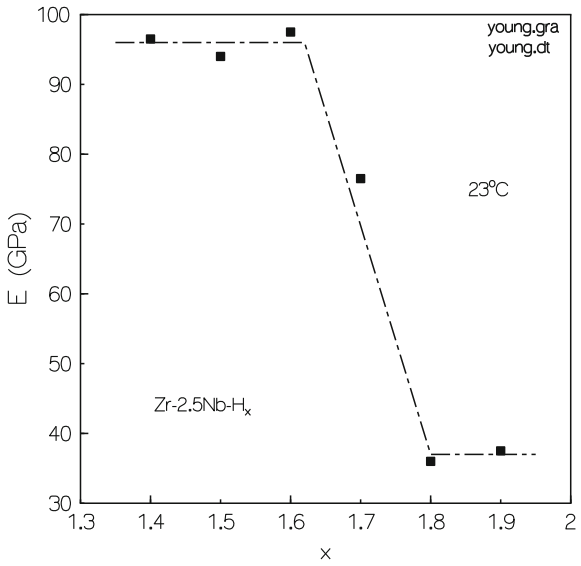

Fig. 2.30 Elastic modulus of Zr-2.5 Nb-H_x (equivalent to ZrH_x) versus $x \equiv r$ at room temperature from unconfined compression tests. The dashed line has been drawn to indicate the trend (from Puls et al. [23]; with permission from AECL)

to a value of 98.15 GPa obtained by Puls et al. using the same value of v. However, since the hcp lattice of the zirconium starter material is elastically anisotropic, differences could result if the indentations in the two types of tests did not sample crystal grains of the same lattice orientation.

Syasin et al. [27] carried out microhardness, elastic modulus, internal friction, and micro-brittleness measurements for bulk hydrides of compositions $ZrH_{1.66}$ to $ZrH_{1.99}$. This composition range starts at what is thought to be approximately the (metastable) equilibrium composition of the δ-hydride phase with the ε-hydride phase and the phase field compositions for the $(\delta + \varepsilon)$- and ε-hydride phase regions of the phase diagram (see Fig. 2.32 further on). Using a Vickers diamond indenter, their room temperature microhardness results show an oscillatory behavior as a function of hydrogen composition, giving an average value of 1.67 GPa with a maximum of 1.72 GPa at $r = 1.94$ and minimum of 1.47 GPa at just below $r \sim 1.9$. These hardness values are much lower than the average value of 3.31 GPa obtained by Xu and Shi [30] for a composition of $ZrH_{1.83}$. E determined by Syasin et al. ranges from 80 to 85 GPa for $r = 1.66$ to just below $r \simeq 1.9$, respectively, then drops abruptly at $r = 1.9$ to $\sim$75 GPa. Similarly, micro-brittleness exhibits a trough at just below $r = 1.9$ followed by a peak at $r = 1.94$ while internal friction has a peak at just below $r = 1.9$. No explanation was offered as to what mechanism could be responsible for the existence of these extrema which were, moreover, found to occur at the same hydrogen composition values.

Yamanaka et al. [31–33] obtained room temperature microhardness and elastic modulus results for solid hydride specimens having hydrogen contents ranging from $r = 1.5$ to 1.68. The upper range of hydrogen content of their specimens is close to the hydrogen content where other workers have observed a sharp

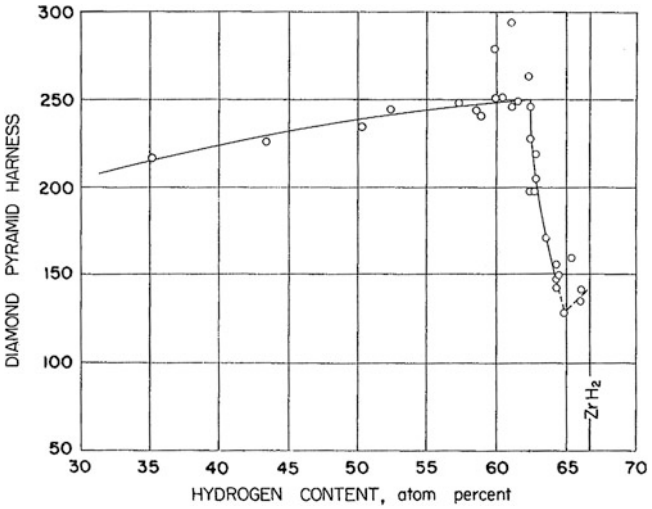

Fig. 2.31 Microhardness versus hydrogen composition (content) of Zr-at.% H (from Beck [7])

reduction in microhardness and other mechanical property values. Beck's [7] data, reproduced in Fig. 2.31, shows the drop off in microhardness values occurring beyond $r = 1.61$ (62.5 at.%) while Barraclough and Beevers' data [5], reproduced in Fig. 2.32, show it to be beyond $r = 1.56$. From the plot of effective elastic modulus, E' obtained by Puls et al. [23], reproduced in Fig. 2.28, the drop off appears to be from $r = 1.51$ to 1.56, although the composition intervals for these data points are very coarse. Still, the drop off would likely not be greater than $r = 1.6$ on the basis of this plot. On the other hand, their corresponding data for the variation of E with r (Fig. 2.30) obtained from the stress–strain curves of their last set of unconfined compression tests—for which it is believed the hydrogen content was more accurately obtained—show the drop off to occur at $r = 1.62$. This drop off with composition is close to that ($r = 1.65$) at which a corresponding drop off in yield strength occurs (Fig. 2.22). Since the latter is derived from the same load–displacement curves, this result is, perhaps, not too surprising. Both Beck [7] and Puls et al. [23] show a slight increase in microhardness or—the equivalent—E′, up to the drop off composition, while the microhardness results of Barraclough and Beevers remain approximately constant up to the drop off composition. These results differ from the microhardness values obtained by Yamanaka et al. (1969a, b) ranging over the composition range from $r = 1.47$ to 1.68 showing a slight linear reduction in microhardness over this composition range, with no indication of a drop off over this range of compositions. These authors claimed that their pellet specimens contained no microscopic cracks or pores. They give the variation of Vickers Hardness, H_v, as:

$$H_v(GPa) = 7.19 - 2.77r \tag{2.8}$$

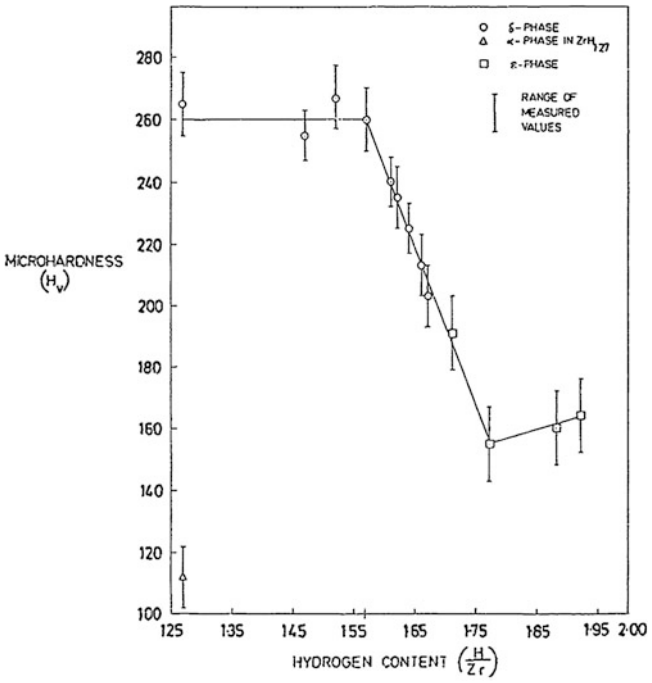

Fig. 2.32 Microhardness versus hydrogen composition (content) $r = \mathrm{H/Zr}$ of $\mathrm{ZrH_r}$ (from Barraclough and Beevers [5])

The value at $r \simeq 1.5$ is ~ 3 GPa. The authors also determined the room temperature elastic modulus, E and shear modulus, G, from measurements of the longitudinal and shear sound velocities for both the hydrogen (protium) and deuterium forms of their solid hydride specimens. The results are reproduced in Figs. 2.33 and 2.34. The authors obtain considerably larger values of E than were obtained by Puls et al. [23] at closely similar hydrogen compositions. One reason for the difference may be because E obtained by Puls et al. is derived from low strain rate tests and would thus represent the isothermal, as opposed to the high frequency, adiabatic, elastic modulus values that are determined by Yamanaka et al. However, Pan and Puls [22], also used a dynamic technique and obtained similar values of E for specimens of composition, $r = 1.5$ as were obtained by Puls et al. One uncertainty is that Yamanaka et al. [31, 32] do not specify the frequency of their sound waves. However, it should be noted that even the results obtained by Syasin et al. are in closer accord with those of Puls et al. [23], Puls and Pan [22] and Xu and Shi [30] than are the values obtained by Yamanaka et al., despite the fact that they are in the hydrogen composition range over which Puls et al. show the elastic modulus has substantially lower values (i.e., for material consisting only of the ε-hydride phase).

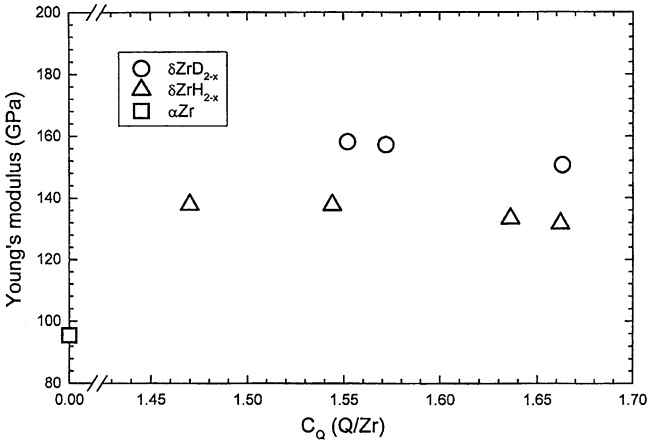

Fig. 2.33 Change in elastic (Young's) modulus, E, of δ-hydride ZrQ_r (Q = D or H; $r \equiv C_Q$) with hydrogen composition, C_Q (from Yamanaka et al. [32])

2.2.4 Summary of Mechanical Strength Results

Overall, comparing the results of Barraclough and Beevers [3–5] with corresponding ones obtained by Puls et al. [23], there are two important differences.

The first difference is that the room temperature yield strength values obtained by Puls et al. are considerably higher than those obtained by Barraclough and Beevers with the highest values of the former being those determined with the Griggs machine under confinement. (It should be noted that differences in yielding behavior as a result of different starting material or hydrogenation temperature were not detectable within the scatter of the results.) Puls et al. obtained room temperature yield strength values ranging from a low of 721 MPa at $r = 1.57$ to a high of 990 MPa at $r = 1.66$, over a hydrogen composition range of $r = 1.4$–1.66, with an average value of 858 MPa. This average value is close to that obtained at room temperature for unhydrogenated Zr-2.5 Nb pressure tube material, although not for the much softer reactor-grade Zr starting material. Since there is little difference in the yield strength values in the foregoing composition range depending on which starting material was used, this means that the yield strength of the hydrogenated material is mainly determined by its lattice structure and hydrogen composition and not from its starting material.

The effect of confinement in increasing the measured average yield strength value over the foregoing hydrogen composition range is further evidenced by comparison with the results of the room temperature tests without confinement. The unconfined tests resulted in an average yield strength value over the composition range from $r = 1.4$ to 1.66 of 611 MPa compared to an average value under confinement of 858 MPa. This amounts to a reduction of $\sim$250 MPa when not using confinement. In comparison, the yield strength values obtained by Barraclough and Beevers, also without confinement, in the composition interval from $r = 1.27$ to 1.66 ranged

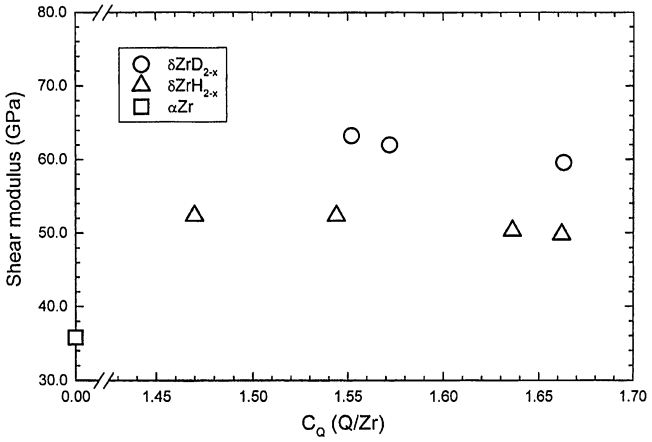

Fig. 2.34 Change in shear modulus, G, of δ-hydride ZrQ_r (Q = D or H; $r \equiv C_Q$) with hydrogen composition, C_Q (from Yamanaka et al. [32])

from ~390 to 250 MPa, respectively. The reason that Barraclough and Beevers' yield strength values are lower may be because their hydrogenation procedure resulted in the generation of a greater number of pre-existing microscopic cracks, the number of these cracks increasing with increasing hydrogen composition. These microscopic cracks could then be controlling the shape deformation of their specimens, resulting in premature fracture at room temperature and softer yielding behavior at higher temperatures compared to the specimens grown by Puls et al. containing possibly fewer, or no, as-grown microscopic cracks and/or made less susceptible to these cracks by testing under confinement.

The second difference is that the plots of yield strength versus temperature obtained by Puls et al. [23] do not exhibit the small maximum in yield strength at ~270 °C obtained by Barraclough and Beevers [3]. A possible reason for this involves the same reasoning used in the foregoing to explain why Barraclough and Beevers' specimens appeared more brittle at room temperature and had a softer load–displacement response at slightly higher temperatures than those obtained by Puls et al. At higher temperatures, the greater ductility of the material would result in the pre-existing microscopic cracks no longer controlling the nonlinear deformation of the material and the proportional limit obtained would more closely reflect the true plastic response of the material. The significantly higher proportional limits obtained by Puls et al. below 100 °C are, then, an indication that their results more accurately reflect the true plastic response of the material, even at room temperature. This would explain why the yield strength values obtained by Puls et al. decrease continuously with temperature, compared to a peak at some intermediate temperature obtained by Barraclough and Beevers [3].

References

1. Ambler J.F.R.: The effect of temperature on the micro-indentation properties of zirconium hydride. Atomic Energy of Canada Ltd, Report AECL-2538, Chalk River, Ontario, Canada (1966)
2. Balagurov, A.M., Bashkin, I.O., Kolesnikov, A.I., et al.: Neutron diffraction determination of the kinetics of the $\varepsilon \rightarrow \delta$ phase transition in $TiD_{0.74}$. Sov. Phys. Solid State **33**, 711–714 (1991)
3. Barraclough, K.G., Beevers, C.J.: Some observations on the deformation characteristics of bulk polycrystalline zirconium hydrides. Part I: The deformation and fracture of hydrides based on the δ–phase. J. Mater. Sci. **4**, 518–525 (1969)
4. Barraclough, K.G., Beevers, C.J.: Some observations on the deformation characteristics of bulk polycrystalline zirconium hydrides. Part II: The deformation of ε–hydrides. J. Mater. Sci. **4**, 802–808 (1969)
5. Barraclough, K.G., Beevers, C.J.: Some observations of the phase transformations in zirconium hydrides. J. Nucl. Mater. **34**, 125–134 (1970)
6. Bashkin, I.O., Malyshev, V.Yu., Myshlyaev, M.M.: Reversible $\gamma \rightarrow \alpha + \delta$ transformation in zirconium deuteride. Sov. Phys. Solid State **34**, 1182–1184 (1992)
7. Beck, R.L.: Zirconium-hydrogen phase system. Trans. ASM **55**, 542–555 (1962)
8. Beck, R.L., Mueller, W.M.: Mechanical properties of solid zirconium hydride. In: Nuclear Metallurgy. Metall. Soc. AIME **III**, 63–66 (1960)
9. Bowman, Jr. R.C., Clark, B.D.: Effects of thermal treatments on lattice properties and electronic structure of ZrH. Phys. Rev. **B31**, 5604–5615 (1985)
10. Cassidy, M.P., Wayman, C.M.: The crystallography of hydride formation in zirconium: I. The $\delta \rightarrow \gamma$ transformation. Metall. Trans. A **11A**, 47–56 (1980)
11. Cassidy, M.P., Wayman, C.M.: The crystallography of hydride formation in zirconium: II. The $\delta \rightarrow \varepsilon$ transformation. Metall. Trans. A **11A**, 57–67 (1980)
12. Douglass D.L.: The metallurgy of zirconium. International Atomic Energy Agency (1971)
13. Eiler E.W., Rau R.C., Tholke W.H. et al.: A metal-hydride system. GE-ANPD document, APEN 444 (1958)
14. Gulbransen, E.A., Andrew, K.F.: Crystal structure and thermodynamic studies on the Zr-H system. J. Electrochem. Soc. **101**, 474–480 (1954)
15. Hon, J.F.: Nuclear magnetic resonance study of the diffusion of hydrogen in zirconium hydride. J. Chem. Phys. **36**, 759–765 (1962)
16. Kolesnikov, A.I., Balagurov, A.M., Bashkin, I.O., et al.: Neutron scattering studies of ordered γ-ZrD. J. Phys: Condensed Matter **6**, 8977–8988 (1994)
17. Kolesnikov, A.I., Balagurov, A.M., Bashkin, I.O.: A real-time neutron diffraction study of phase transitions in the Ti-D system after high-pressure treatment. J. Phys: Condensed Matter **5**, 5045–5058 (1993)
18. Libowitz, G.G.: A pressure-composition-temperature study of the zirconium-hydrogen system at high hydrogen contents. J. Nucl. Mater. **5**, 228–233 (1962)
19. Mogilyanskii, D.N., Bashkin, I.O., Degtyareva, V.F., et al.: Sov. Phys. Solid State**32**, 1039–1041 (1990)
20. Moore, K.E., Young, W.A.: Phase studies of the Zr-H system at high hydrogen concentrations. J. Nucl. Mater. **27**, 316–324 (1968)
21. Numakura, H., Koiwa, M., Asano, H., et al.: Neutron diffraction study of the metastable γ titanium deuteride. Acta Metall. **36**, 2267–2273 (1988)
22. Pan, Z.L., Puls, M.P.: Internal friction peaks associated with the behaviour of hydrogen in Zr and Zr-2.5 Nb. Mater. Sci. Eng. **A442**, 109–113 (2006)

23. Puls, M.P., Shi, S.Q., Rabier, J.: Experimental studies of mechanical properties of solid zirconium hydrides. J. Nucl. Mater. **336**, 73–80 (2005)
24. Sidhu, S.S., Murthy, N.S.S., Campos, F.P., et al.: Neutron and X-ray diffraction studies of nonstoichiometric metal hydrides. Adv. Chem. Ser. **39**, 87–98 (1963)
25. Simpson, L.A., Cann, C.D.: Fracture toughness of zirconium hydride and its influence on the crack resistance of zirconium alloys. J. Nucl. Mater. **87**, 303–316 (1979)
26. Singh, R.N., Ståhle, P., Massih, A.R., et al.: Temperature dependence of misfit strains of δ-hydrides of zirconium. J. Alloys and Comp. **436**, 150–154 (2007)
27. Syasin, V.A., Boyko, E.B., Markin, V.Ya.: Investigations of hardness, internal friction and brittleness of zirconium hydride. Zeitschrift für Physikalische Chemie Neue Folge **164**, 1567–1572 (1989)
28. Vaughan, D.A., Bridge, T.R.: High temperature X-ray diffraction investigation of the Zr-H system. J. Metals **85**, 528–531 (1956)
29. Veyssiere, P., Rabier, J., Jaulin, J.L., et al.: Instrumental modifications for compressive testing under hydrostatic confining conditions. Rev. Phys. Appl. **20**, 805–811 (1985)
30. Xu, J., Shi, S.Q.: Investigation of mechanical properties of ε–zirconium hydride using micro- and nano-indentation techniques. J. Nucl. Mater. **327**, 165–170 (2004)
31. Yamanaka, S., Yoshioka, K., Uno, M., et al.: Thermal and mechanical properties of zirconium hydride. J. Alloys Compd **293–295**, 23–29 (1999)
32. Yamanaka, S., Yoshioka, K., Uno, M., et al.: Isotope effects on the physicochemical properties of zirconium hydride. J. Alloys Compd **293–295**, 908–914 (1999)
33. Yamanaka, S., Kazuriho, Y., Kurosaki, K., et al.: Characteristics of zirconium hydride and deuteride. J. Alloys Compd **330–332**, 99–104 (2002)
34. Zuzek, E., Abriata, J.P., San-Martin, A., et al.: H-Zr (hydrogen-zirconium): phase diagrams of binary hydrogen alloys, pp. 309–322. ASM International, Ohio (2000)

http://www.springer.com/978-1-4471-4194-5

The Effect of Hydrogen and Hydrides on the Integrity of Zirconium Alloy Components
Delayed Hydride Cracking
Puls, M.P.
2012, XXXII, 452 p., Hardcover
ISBN: 978-1-4471-4194-5